Mesoscopic modeling of the impact behavior and fragmentation of porous concrete

Agar Ozbek, Ayda Safak; Pedersen, Ronnie Refstrup; Weerheijm, Jaap; van Breugel, Klaas

Citation (APA)
Agar Ozbek, A. S., Pedersen, R. R., Weerheijm, J., & van Breugel, K. (2019). Mesoscopic modeling of the impact behavior and fragmentation of porous concrete. *Cement and Concrete Composites*, *102*, 116-133. https://doi.org/10.1016/j.cemconcomp.2019.04.020

Important note
To cite this publication, please use the final published version (if applicable).
Please check the document version above.

Mesoscopic Modeling of the Impact Behavior and Fragmentation of Porous Concrete

Ayda Safak Agar Ozbek[a,*], Ronnie Refstrup Pedersen[b,c] Jaap Weerheijm[d,e], Klaas van Breugel[d]

[a] Faculty of Civil Engineering, Istanbul Technical University, Istanbul, Turkey
[b] Department of Civil Engineering, Aalborg University, Esbjerg, Denmark
[c] Rambøll Offshore Wind, Esbjerg, Denmark
[d] Faculty of Civil Engineering and Geosciences, Delft University of Technology, Delft, The Netherlands
[e] TNO, Defense, Security and Safety, Rijswijk, The Netherlands

Abstract

This study presents the numerical analyses conducted to investigate the impact behavior of different porous concretes, which have also been cast and tested experimentally. For a realistic representation of the real porous concretes containing arbitrary shaped air pores, a mesh generation code was developed in which the aggregates in the mixtures were directly extracted through computed tomography. In the code, mineralogically different aggregates in porous concretes with gravel could also be individually defined. In the explicit finite element analyses conducted, porous concrete was considered as a four-phase material, consisting of aggregates, interfacial transition zones (ITZ), bulk cement paste and air. The pore size distribution and the fragmentation behavior of the concretes were also numerically analyzed. Among the parameters that have been investigated both numerically and experimentally, aggregate grading, which determines the porosity and pore size distribution of the material, was found to have a dominant effect on the strength as well as the fragmentation properties of porous concretes. Although the amount of ITZ is higher in mixtures containing finer aggregates, those mixtures had higher impact strengths compared to coarser aggregate ones again owing to their much finer pore structures.

1. Introduction

Numerical simulation techniques play an increasingly important role in designing and investigating cementitious materials. Different numerical methods are used by researchers for simulating the behavior of cementitious materials in a realistic way where the outcome is also verified with experimental results [1-4]. This study aims to simulate and assess the dynamic behavior of different porous concretes under impact loading, which also constitutes a part of a research project with safety and security purposes. The motive behind the project was that when an explosion takes place close to or inside a concrete structure, in addition to the dangers of the explosive itself, the hazard due to the flying debris from the concrete construction is a very important threat. Therefore, a type of cementitious material, which fractures into small fragments under impact loading while having sufficient static strength to be used as a building material, was aimed to be developed. In the scope of the project, different types of concretes were investigated while enhanced strength porous concretes (reaching 50 MPa static compressive

strength) fracturing into small size fragments under impact loading were developed by adjusting the mixture composition and highly compacting the sample by also using a set retarder [5]. In the currently presented study, numerical simulations, conducted during the material development process, for predicting and better understanding the dynamic response as well as the fragmentation properties of porous concretes are presented. The numerical results were also used to obtain a research direction to follow.

Porous concrete is designed for intentionally high volumes of meso-size air pores and is efficiently used in various applications mainly owing to its permeability and insulation properties. [6-11]. Pores, in return, are among the major determinants of the mechanical properties of porous materials. In the numerical analyses, the distinctive properties of porous concretes compared to normal concrete are therefore the presence of arbitrary shaped meso-scale air pores and the coalescence of the free surfaces of the pores as the loading proceeds [5]. Another major difference between normal concrete and highly compacted porous concrete is that porous concrete contains a continuous network of coarse aggregates from bottom to top which functions as a skeleton that enhances the strength of the material. Therefore, it has a higher coarse aggregate volume compared to normal concrete.

2. Numerical Analyses of Real Porous Concretes

In this work, real porous concrete mixtures, which have been experimentally produced and tested, were analyzed numerically. The numerical output could therefore be compared with experimental results. The work comprises (i) the aggregate particle distribution and mesh generations performed by the codes developed, (ii) the finite element analyses conducted with a general purpose finite element program ABAQUS/Explicit and (iii) pore and fragment size distribution analyses.

In the analyses, explicit time integration method was used. The explicit integration scheme is available in ABAQUS/Explicit (explicit dynamic analysis module). Explicit finite element analysis techniques are currently adopted for various applications that involve highly nonlinear systems with large deformations and rotations, extensive contact and/or impact. The explicit scheme is a problem solving method and different from implicit methods, it is incremental, but not iterative [12-14]. In general, implicit and explicit integration methods have their own advantages and disadvantages. In the explicit methods, the computational cost per time step is less than implicit methods, which is an important advantage. However, an explicit method is only conditionally stable. Since no iterations are performed, small time increments are essential to ensure acceptable results. Therefore, such methods are more applicable when the time step size required for stability is feasible to describe the physical problem, which is usually the case in wave propagation analyses [12-15]. Therefore, for dynamic analyses of short duration incidents, explicit methods are efficiently being used [14, 16-18]. In this study, explicit time integration has been selected as the analysis method because of the high nonlinearity of the system as well as the short duration of loading.

2.1. Finite Element Mesh Generation

Mesoscopic analysis of porous concrete requires the generation of a random aggregate structure in which the size, shape and spatial distributions of the coarse aggregate particles resemble those of real porous concretes. On the other hand, the presence of the arbitrary shaped meso-scale air pores is another important factor that should be considered in the numerical analyses. Therefore, a mesh generation code was written in MATLAB for generating realistic meshes for porous concretes. Computed tomography (CT) was used in mesh generation both in determining the aggregate distribution (see Fig. 1) and in quantifying the porosity of the porous concrete specimens. In the CT image, different materials are indicated by different shades of gray according to their densities. In the CT scans of porous concretes on the other hand, because the densities of the aggregates and the cement paste were not drastically different, it was not possible to clearly visualize the outer borders of the aggregate particles. For mesh generation, the coordinates of the aggregate borders were required. Using that data on the borders of the aggregates (the blue borders in Figs. 1 and 2) and by defining thicknesses for ITZ and bulk cement paste phases, the outer borders of ITZ (green borders) and cement paste (red borders) were numerically generated as shown in Figs. 1 and 2. To be able to determine the coordinates of the aggregate borders, all the porous concrete mixtures that had been planned to be numerically analyzed, were cast again by using a high viscosity epoxy based resin instead of cement paste. The aggregate content and the production method (placing and compaction) were kept exactly the same as in real porous concrete mixtures. Owing to the low density of the epoxy resin (about 1.14 g/cm^3), which became the new matrix, a much larger difference between the densities of the matrix and the aggregates, i.e. a clearer distinction in the CT images, was possible, as can also be seen in the CT images in Figs. 1 and 3. In the program, by converting the gray scale CT images to binary (black and white) and then by finding the coordinates of the borders of aggregates, each aggregate grain was defined and numbered individually.
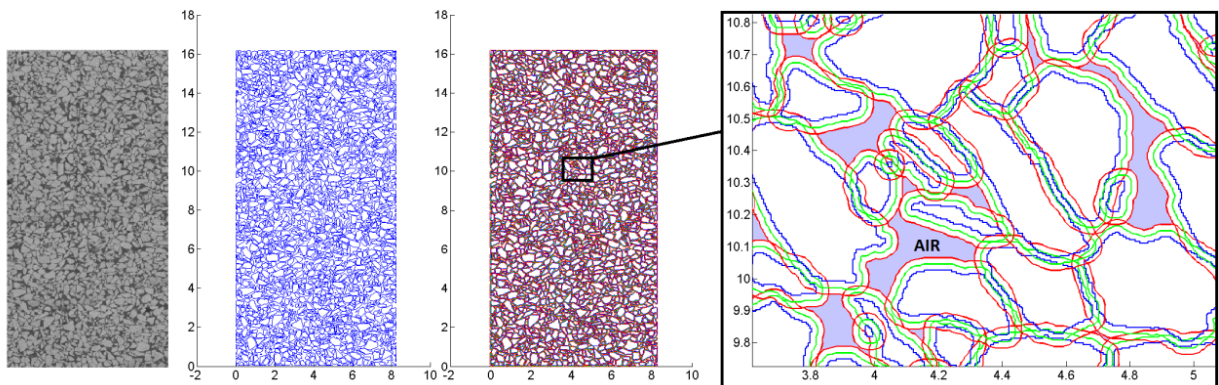

Fig. 1. (Left) CT image of a 2-4 mm basalt aggregate epoxy porous concrete, (middle) the detected borders of the aggregates, (right) borders of the phases: aggregates (blue), ITZ (green) and bulk cement paste (red)
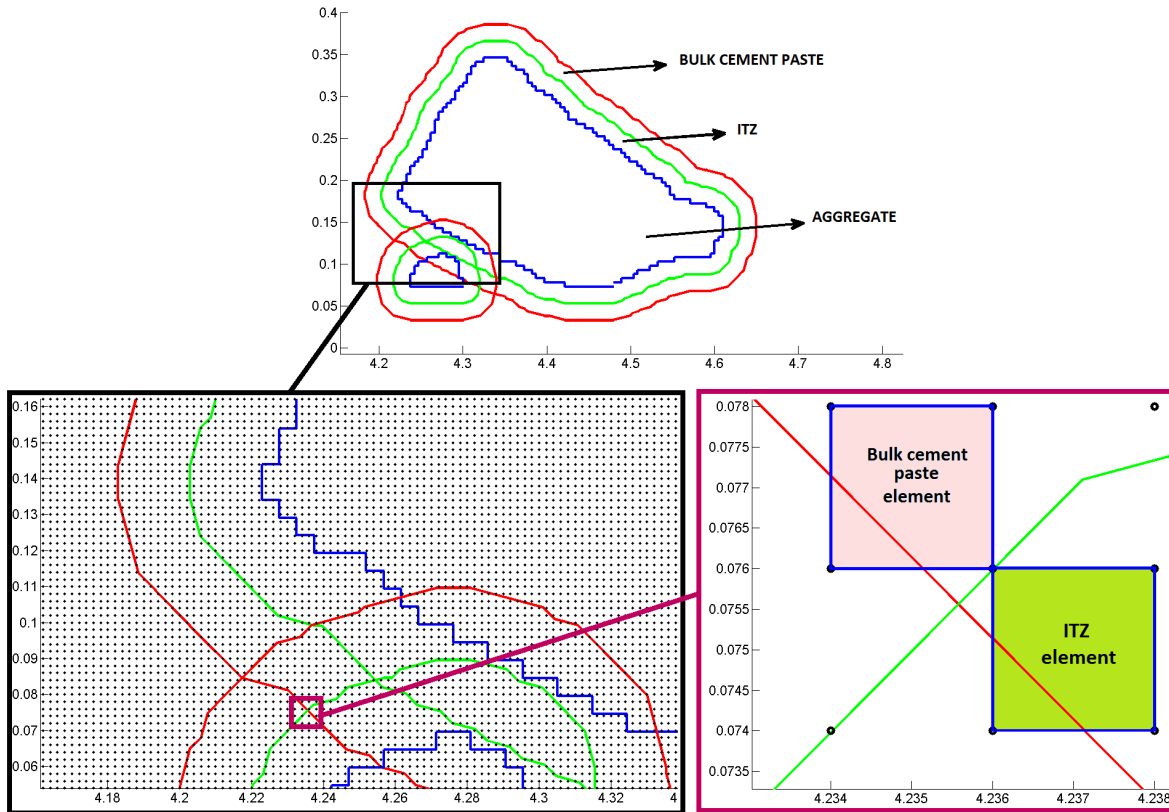
Fig. 2. Mesh generation- categorizing the elements of a background mesh

After the program created three sets of borders, representing the borders between the four phases i.e. aggregate, ITZ, bulk cement paste and air (blue, green and red borders in Figs. 1 and 2), a background mesh was generated. Initially, all the nodes of the background mesh were checked one by one, based on which borders they were located in, according to their coordinates. Afterwards, each element was checked in accordance with how many of its nodes were located in which material phase. The element having the majority of its nodes in one phase was assigned by the properties of that specific material phase. If the nodes of the element were equally placed in more than one material, the phase closer to the aggregates i.e. in the order starting from aggregates to ITZ, cement paste and air, is selected. The rest of the elements were assigned by the air phase. After all the elements were distributed to the respective phases, the porosity was checked by counting the elements of air phase. If the porosity was found to be sufficient, the air elements as well as the nodes belonging to only the air phase were completely removed from the mesh. A finite element mesh generated using a section from a porous concrete made with epoxy resin is presented in Fig. 3.
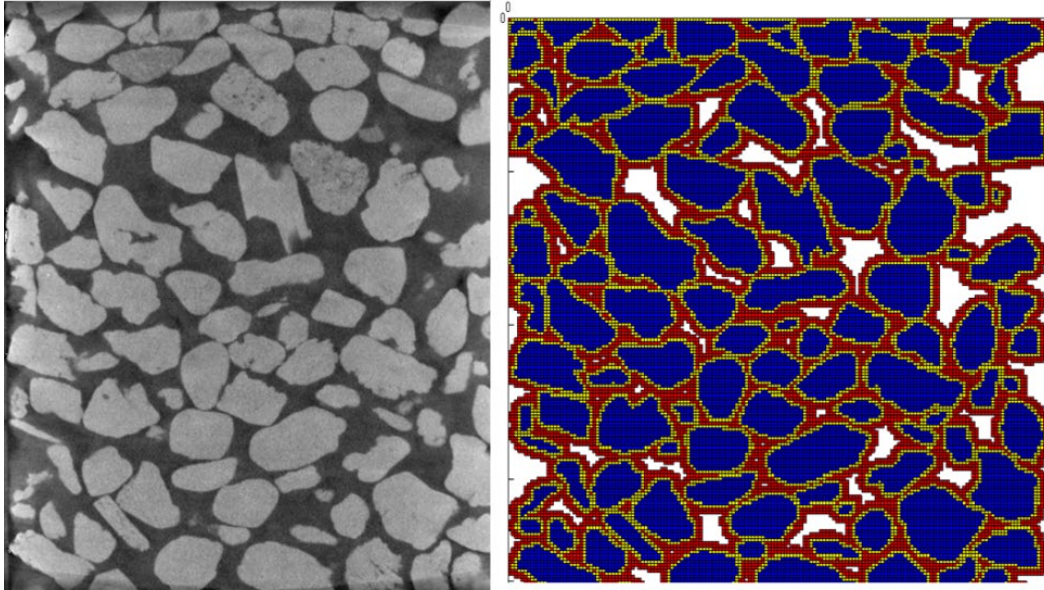
Fig. 3. Mesh generation using CT scan: a) (left) CT image of a porous concrete with 4-8 mm gravel aggregates produced with epoxy resin, b) (right) the respective porous concrete mesh generated

Measuring the meso-size porosity of the mixtures, which was taken as reference in mesh generation as the target porosity, was done by converting the acquired images of a real porous concrete sample to binary mode. An example is shown in Fig. 4. By using the image processing toolbox of MATLAB, the ratio of the solid and air phases, i.e. the numbers of black and white pixels, is determined. Based on the aimed porosity, the thickness of the cement paste phase is adjusted in the main mesh generation computation by trial and error. After an approximately close value is reached for a mesh, the small adjustments are done this time by using the trimming option seen in Fig. 5.
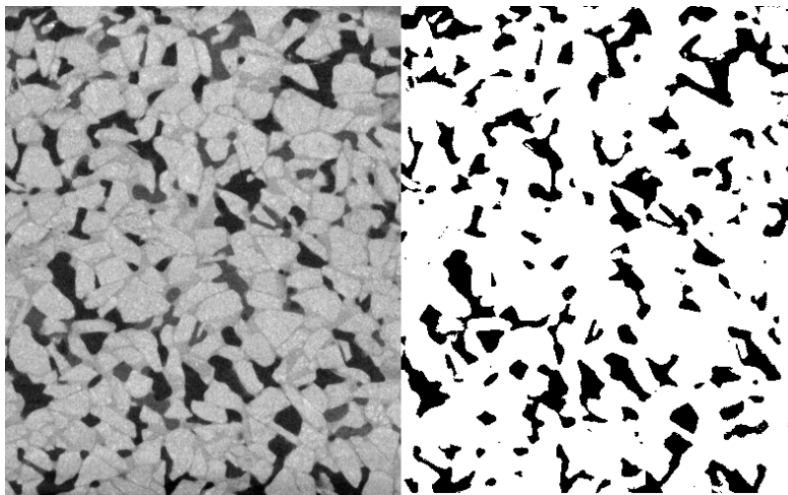

Fig. 4. Determination of porosity: a) (left) CT image of a section, b) (right) Image converted to binary mode

In order to adjust the porosity as well as to form a realistic distribution of cement paste phase, locally trimming the outer layer of bulk cement paste elements was also needed during mesh generation. This is illustrated in Fig. 5, where the original mesh at the top is trimmed by progressively removing the cement paste elements that have two or more free surfaces (indicated with the same colors) step by step until the aimed amount of porosity is reached. Similarly, in real porous concretes the actual thickness of cement paste is not uniform around the aggregates. At free surfaces (marked with red), the cement paste layer gets slightly thinner while at contact locations (marked with blue) the thickness of the cement paste is much higher.
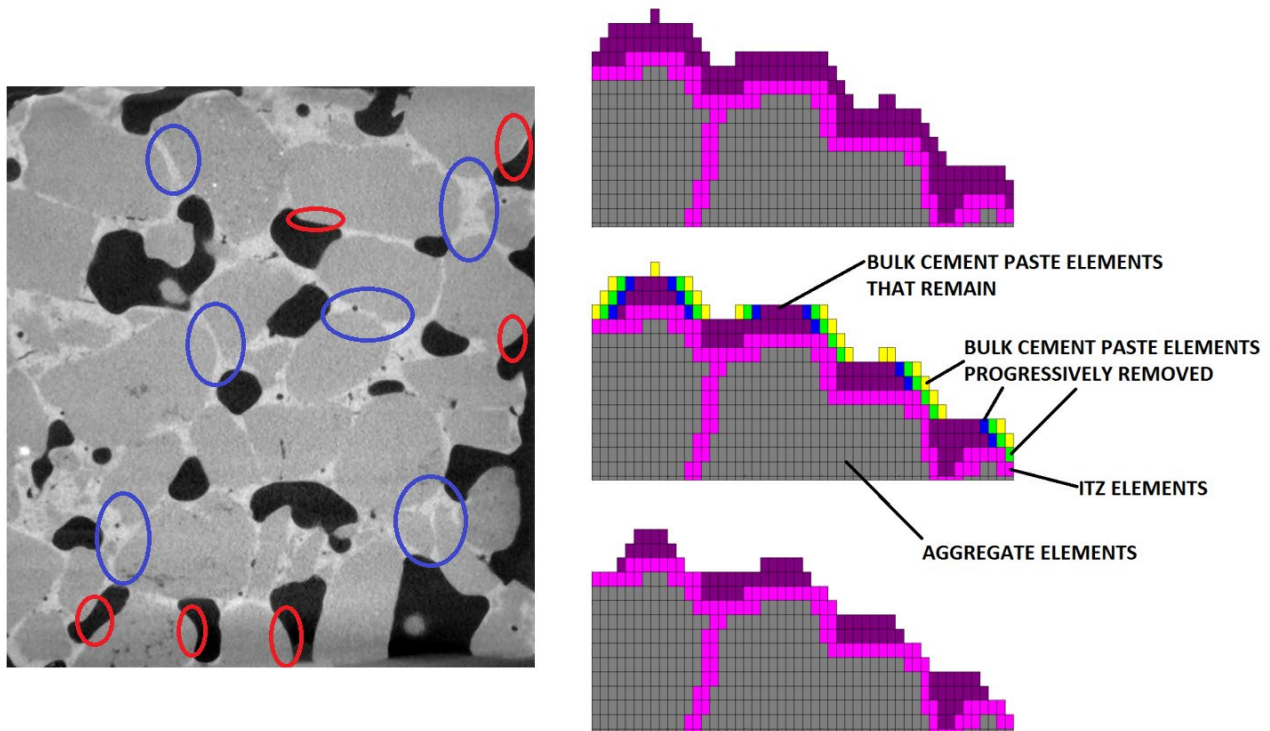

Fig. 5. (Left) CT image of a real porous concrete, (Right) Progressive trimming of the cement paste elements in mesh generation (from top to bottom) initial configuration, intermediate configurations subject to removal of bulk paste elements, final configuration meeting the target porosity

2D Axisymmetric geometry is used in the analyses. The drop weight impact test setup that is defined in the simulations consisted of a stationary steel base structure at the bottom, the cylindrical concrete sample and the steel impactor. A typical finite element mesh showing the test set-up is presented in Fig. 6. The dimensions of the mesh representing the concrete sample was 30 mm in width and 75 mm in height (corresponding to 60 mm diameter, 75 mm height sample when rotated axisymmetrically). The mesh for the steel impactor was 55 x 220 mm (corresponding to 110 mm diameter and 220 mm height). In Figs. 6, 7 and 8, half of the section, that is rotated axisymmetrically, is shown for the different porous concrete mixtures analyzed.

6

The steel impactor parts of the mesh are mostly cropped from the images. The elements were 0.2 mm x 0.2 mm four-node, reduced integration, axisymmetric elements (CAX4R in ABAQUS).

The analysis of the impact behavior of a cylindrical porous concrete sample is actually a three dimensional problem. However, because of the restrictions due to 2D mesh generation i.e. due to the mesh generation being performed based on the detailed image analysis of 2D sections selected from the computed tomography scans of real concretes, and because the number of elements for representing a two dimensional section currently reaches about 200000 elements (including the impactor and the steel base structure), an axisymmetric analysis had to be preferred also considering the limitations of computer power. In the analyses, it is recommended to have similar size elements at the two surfaces of contact with friction, in order not to have additional problems due to contacts [25]. For that purpose, the meshes for the steel components of the setup were also selected to be approximately as fine as the meshes for the concrete sample. Meanwhile, the meshes of porous concrete samples were generated to be very fine in order to capture the interfacial transition zone (ITZ) phase, which is at the micrometer scale. Considering all the features of the analysis, the model was therefore selected to be 2D axisymmetric. Axisymmetric models represent a slice that is revolved 360 degrees around the y axis of the reference Cartesian coordinate system. All the included geometry must lie in the positive x portion of the xy plane. The geometry used in the analyses was a section taken from the porous concrete impact testing setup as seen in Fig.6.
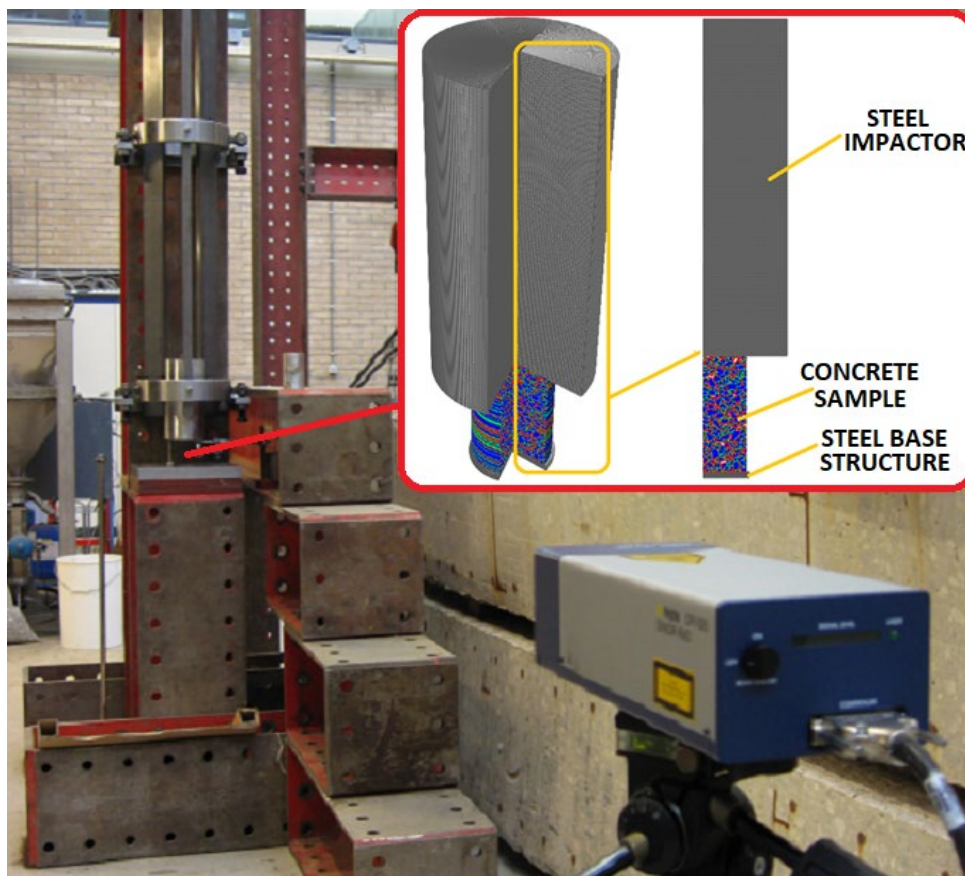
Fig. 6. Test set-up and finite element mesh for the impact analysis of porous concrete
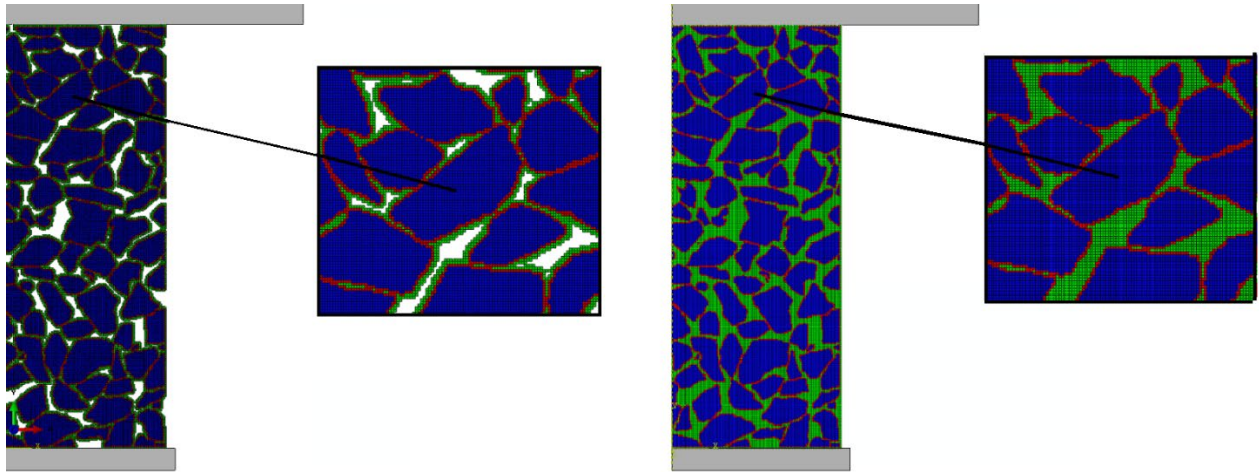

Fig. 7. Finite element meshes for 4-8 mm basalt porous concrete (PRC1 in Table 3) and 4-8 mm basalt full concrete (FC1)
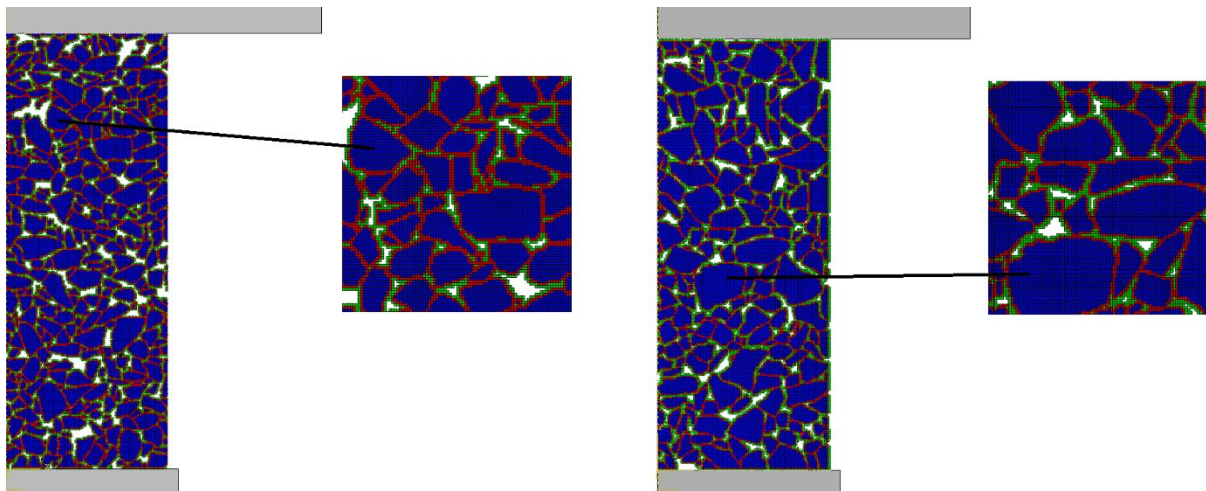

Fig. 8. Finite element meshes for 2-4 mm (PRC2 in Table 3) and 50% 4-8 mm-50% 2-4 mm basalt (PRC3) porous concretes

In the scope of the research project, with the aim to design porous concretes that fracture into small fragments and have relatively high static strength, a sensitivity study was conducted where many factors that affect the properties of porous concrete were investigated. In the process of improving the material properties, enhancing the static strength while maintaining the porous structure was the main aim. Starting from porous concretes with very low static compressive strengths, by modifying the mixture composition as well as the method of compaction, porous concretes with enhanced static strengths (at the range of 30-50 MPa) were designed and experimentally produced. The main features of the process of enhancing the strength properties

of porous concrete in the research project are presented in Fig. 9, where the static compressive strengths of some selected porous concrete mixtures are summarized [5]. While some of the lower strength mixtures were also numerically analyzed (using another software and implicit analysis), the main focus of the explicit numerical analyses presented in this paper was the higher strength and more promising mixtures (two of which are the highest two curves in Fig. 9 i.e. PRC1 and PRC3 in this paper) to see the effects of especially the aggregate and pore size distributions on the behavior of porous concretes.
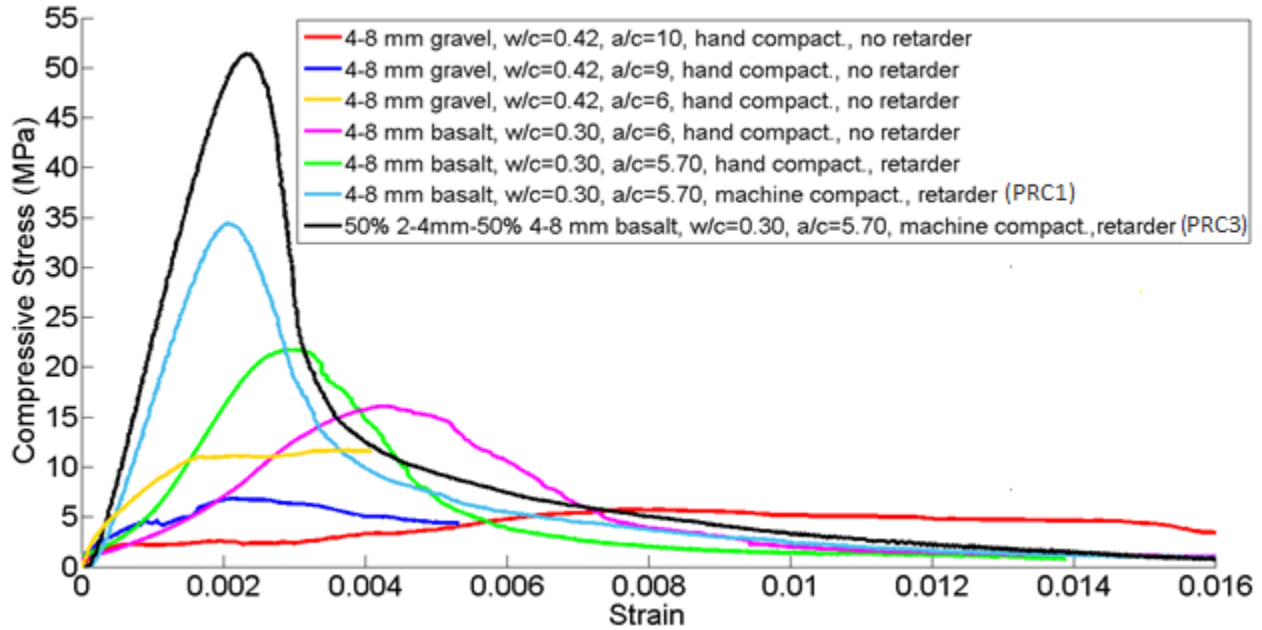

Fig. 9 Static compressive strengths of selected porous concrete mixtures

Experiments at different scales were performed to determine the effectiveness of the various factors while the outcome of the tests as well as the numerical analyses guided the process of modification of the material. The compositional properties of the experimental porous concrete mixtures and a full concrete, that have also been analyzed numerically, and a moderate strength normal concrete mixture cast for comparison are presented in Tables 1 and 2. In Table 1, the amounts per specimen was given because in the production, specimens were mixed, cast and compacted individually.

Table 1. Compositional properties of porous concrete and the full concrete mixtures

Mixture code	PRC1	PRC2	PRC3	PRC4	FC1
Crushed basalt (2-4 mm) (gr)	-	2000	1000	-	-
Crushed basalt (4-8 mm) (gr)	2000	-	1000	-	2000
River gravel (4-8 mm) (gr)	-	-	-	2000	-
Cement (gr)	351	351	351	351	951

9

Water (gr)	105	105	105	105	285
Superplasticizer (gr)	0.97	0.97	0.97	0.97	4.20
Set retarder (gr)	1.20	1.20	1.20	1.20	2.22

Table 2. Compositional properties of the normal concrete mixture (NC1)

NC1 composition	Amounts (g per 2.5 dm^3)
CEM I 42.5N	1033
0.125-0.250 mm sand	440
0.250-0.500 mm sand	813
0.500-1 mm sand	940
1-2 mm sand	940
2-4 mm sand	1253
4-8 mm river gravel	1880
Water	583
Superplasticizer	19

Table 3. Analyses conducted on real porous concretes and the experimental strength results

REAL POROUS CONCRETES Material Phases: Aggregates + ITZ + Bulk Cement Paste + Air (except FULL4-8)					
			Experimental Results		
Mixture Code	Analysis Label	Aggregates	Meso-scale Porosity (Image Analysis, Fig.4)	Experimental Static Strength (MPa)	Experimental Impact Strength (MPa)
PRC1	BASALT4-8	4-8 mm basalt	21.8	34.78	66.52
PRC2	BASALT2-4	2-4 mm basalt	20.3	41.89	76.78
PRC3	BASALT2-8	50% 2-4 mm – 50% 4-8 mm basalt	18.8	50.49	85.99
FC1	FULL4-8	4-8 mm basalt	0	61.10	-
PRC4	GRAVEL4-8	4-8 mm river gravel	17.9	29.64	56.22
NC1	-	continuously graded gravel	0	26.44	57.97

Full concrete (FC1) specimens were experimentally produced by completely filling and vibrating the porous concrete sample with cement paste just after compaction, at the fresh state. Therefore, the sample is different from normal concrete in the sense that there is still no fine aggregates involved. It is essentially a porous concrete sample where all the meso-scale air pores are filled with cement paste. This mixture, which has a quite higher strength compared to porous concretes as expected, was used in investigating the effect of the lack of pores in the behavior of the material by comparing the evolution of impact stresses as well as the fracture patterns. The moderate strength normal concrete (NC1) on the other hand, is a conventional concrete produced with continuously graded aggregates. The reason for including this mixture in the research was comparing the fragmentation of a normal concrete, having approximately similar strength properties as a moderate strength porous concrete, with the fragmentation of porous concretes. The fragmentation behavior, which was one of the main parameters investigated in the research, was compared for normal and porous concretes to be able to see the benefits of porous concrete in decreasing the fragment size. The main features of the numerical analyses conducted on the selected concrete mixtures and their experimental strength results are given in Table 3 [20].

Along with macro-scale tests, in order to understand the global behavior of a composite material, the properties of its different phases should be investigated separately at a lower scale. Because the model includes four different material phases (three solid phases and air), input for all the three phases were required. Therefore, data on the mechanical properties of the interfacial transition zone (ITZ) was essentially obtained by performing meso-scale tests. The meso-scale ITZ testing was conducted in the scope of the experimental part of the research [5, 20]. In the meso-scale ITZ testing, to be able to have samples with as realistic ITZ phases as possible, the natural rough surfaces of aggregates were preserved. For that purpose, natural aggregates (basalt or different types of river gravel), with an 8 mm by 8 mm square cross-section, were used, taking the 4-8 mm aggregate size range of the porous concrete as reference. The size of the cement paste parts of the samples were therefore, comparable with the cement paste bridges present between the aggregates in porous concrete samples. Owing to this, the cement paste in the samples was affected by similar conditions in terms of shrinkage. The aggregates with square shaped cross sections were cut from the special aggregate-glue composite samples (see Fig. 10, the top right image). Aggregate-glue composite samples were prepared using an epoxy based low viscosity glue at the bottom to be able to have a horizontal surface on top, while having the flat surface of the glue at the bottom. ITZ samples were then cast by pouring cement paste onto square aggregates in steel molds.

While most of the porous concrete mixtures in this study contain basalt as the aggregate phase, some mixtures contained river gravel. River gravel naturally consists of a blend of different mineralogical types of rocks, which also have very different levels of adherence to cement paste. The meso-scale tests were conducted using a micro tension-compression testing device (by Kammrath & Weiss) with a 50 N load cell. Closed loop displacement controlled meso-scale tests were conducted on composite samples consisting of aggregate (either basalt or different types of river gravel), cement paste and the ITZ phase formed in between. In all the composite ITZ

samples tested, the failure occurred in the immediate vicinity of the aggregate, which showed that the failure happened at the ITZ. Therefore, the peak load that is measured could be used to determine the tensile strength of the ITZ phase. It should also be noted that due to the different amounts of glue, that is used to prepare and fix the samples, and different aggregate heights, the displacement values are insignificant and cannot be compared with each other [5, 20].
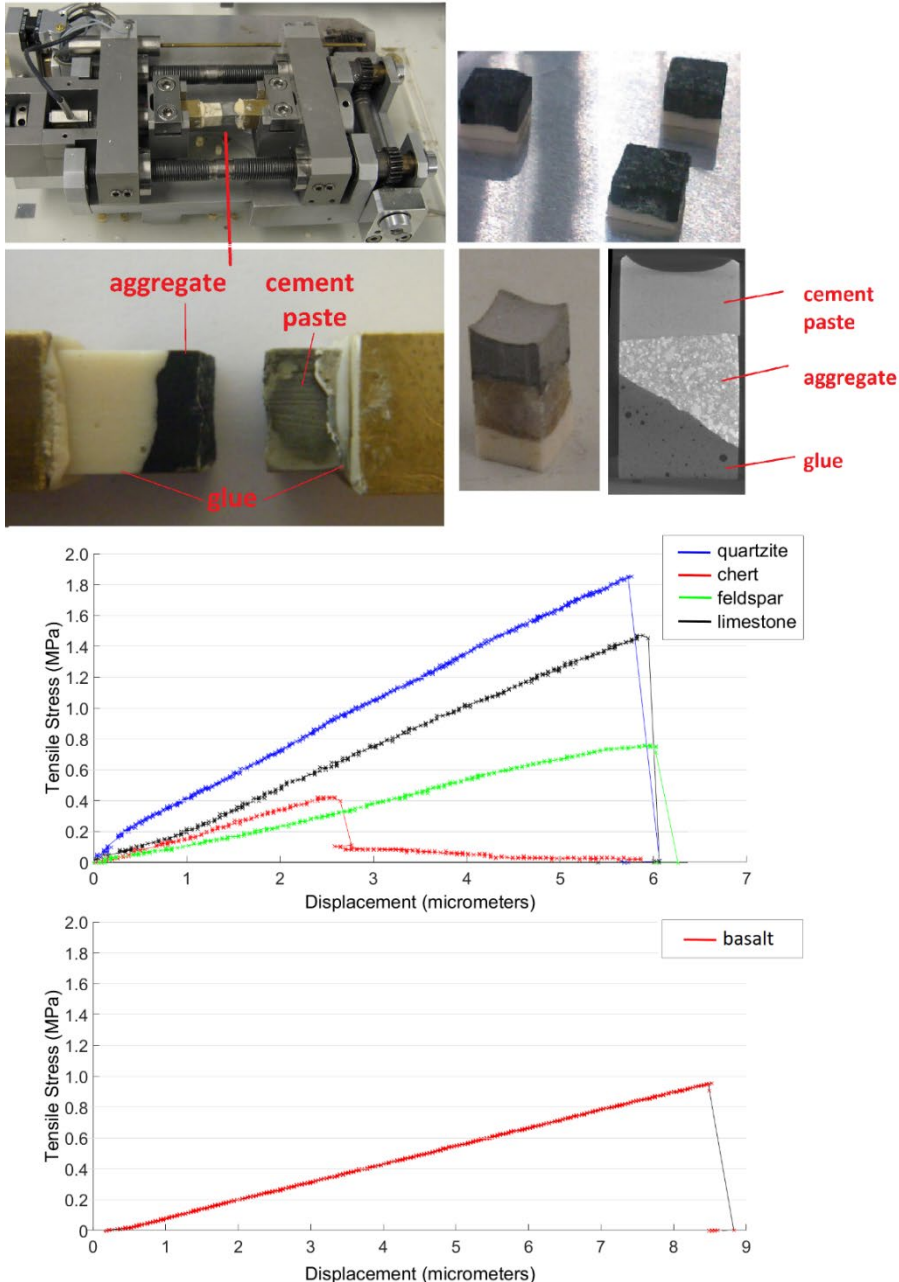

Fig. 10. Meso-scale test set-up, composite ITZ samples of gravel and basalt, the CT image of a composite sample and representative test results for ITZ phases formed between cement paste-different gravel aggregates (middle) and basalt (bottom)
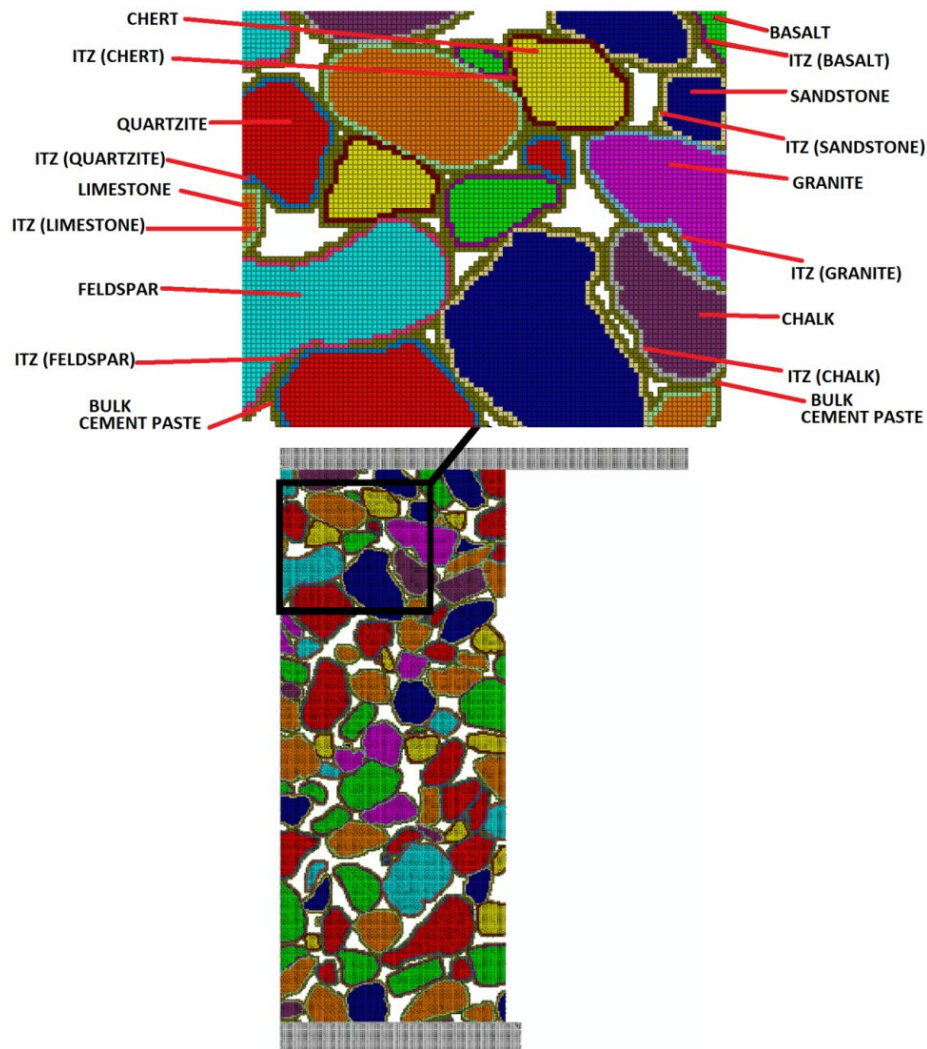
Fig. 11. Finite element mesh for 4-8 mm gravel porous concrete containing different types of gravel aggregates (PRC4 in Table 3)

In the meso-scale mechanical tests conducted on the 4 mm x 4 mm cross-section composite ITZ samples (see Fig. 10), the properties of the ITZ phases were found to be highly varying depending on the type of aggregate [20]. The results of some selected representative tensile tests are presented in Fig. 10. Similarly, it was observed during concrete casting and compaction that some gravel aggregates were very weak compared to the others and that some of them (e.g. chalk aggregates) even fractured during the compaction process. Therefore, in the numerical analyses on gravel porous concrete, different mechanical properties were assigned to the different gravel aggregates and to the corresponding ITZ phases formed around them (see Fig. 11). Because in the mesh generation process, each aggregate grain and each respective phase is defined separately, assigning different properties was possible. Meanwhile, in the mixtures containing basalt, the ITZ properties were also defined using the meso scale test results.

When the distributions of the cementitious phases (bulk cement paste and ITZ elements) in the three porous concrete mixtures containing basalt aggregates (2-4 mm, 4-8 mm, 50% 2-4 mm – 50% 4-8 mm basalt aggregate porous concretes) were compared by simply quantifying the numbers of elements belonging to these phases, the ratios in Fig. 12 were found. The ratio of ITZ elements to aggregate elements (ITZ/AGG) increasing with the decrease in aggregate size (from 4-8 mm to 2-4 mm) was as expected. On the other hand, the ratio of bulk cement paste elements to aggregate elements (CP/AGG) decreasing as the aggregate size was decreased, is due to the mentioned element trimming procedure during mesh generation, in order to increase the porosity and prevent the fine aggregate mixtures to be less porous than the others. In Fig. 12, the ITZ and CP elements in different mixtures are indicated separately by red.
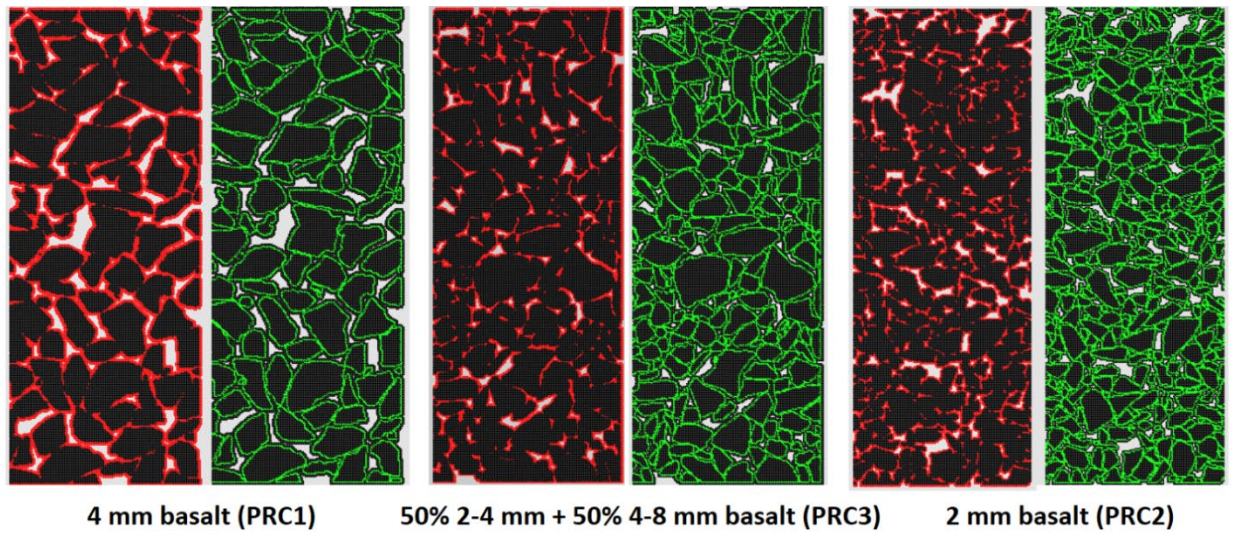
4 mm basalt (PRC1)   50% 2-4 mm + 50% 4-8 mm basalt (PRC3)   2 mm basalt (PRC2)
CP/AGG=27.08% ITZ/AGG=23.33%   CP/AGG=26.28% ITZ/AGG=32.59%   CP/AGG=24.01% ITZ/AGG=45.80%

Fig. 12. Distributions of bulk cement paste (CP) and ITZ phases in different mixtures

2.2. Pore Size Distribution Analysis

Determining the pore size distribution was important for providing complementary information in view of understanding the behavior of porous concretes. Image analysis techniques were used to determine the pore sizes of the mixtures, that have been numerically analyzed, and a short program was written for the purpose. Similar to the analyses performed for determining the real aggregate distributions of porous concretes, the meshes were converted to binary images. The borders of all the pores were defined by checking the black pixels that are neighbors to white (see Fig. 13). Therefore, the border pixels of all the pores have been detected. Subsequently, each border pixel is again checked in terms of being neighbors to other border pixels to continue tracing the complete border of each pore one by one. When all the pores are separately detected, their areas are also calculated in terms of pixels and converted to metric units. In the analysis the pores that are in contact i.e. that share a common black pixel are taken collectively as the same pore. For the pores to be separately defined, there should be at least one layer of white pixels isolating them.
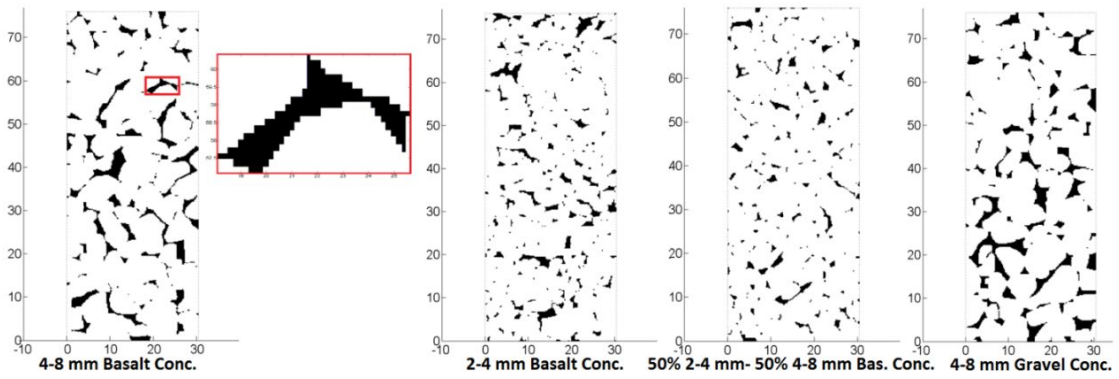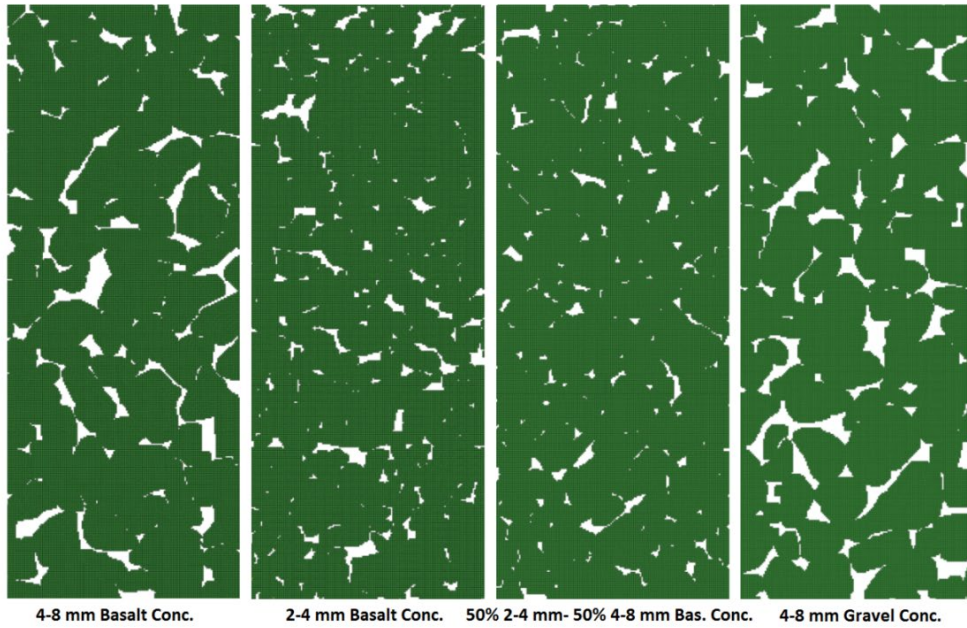
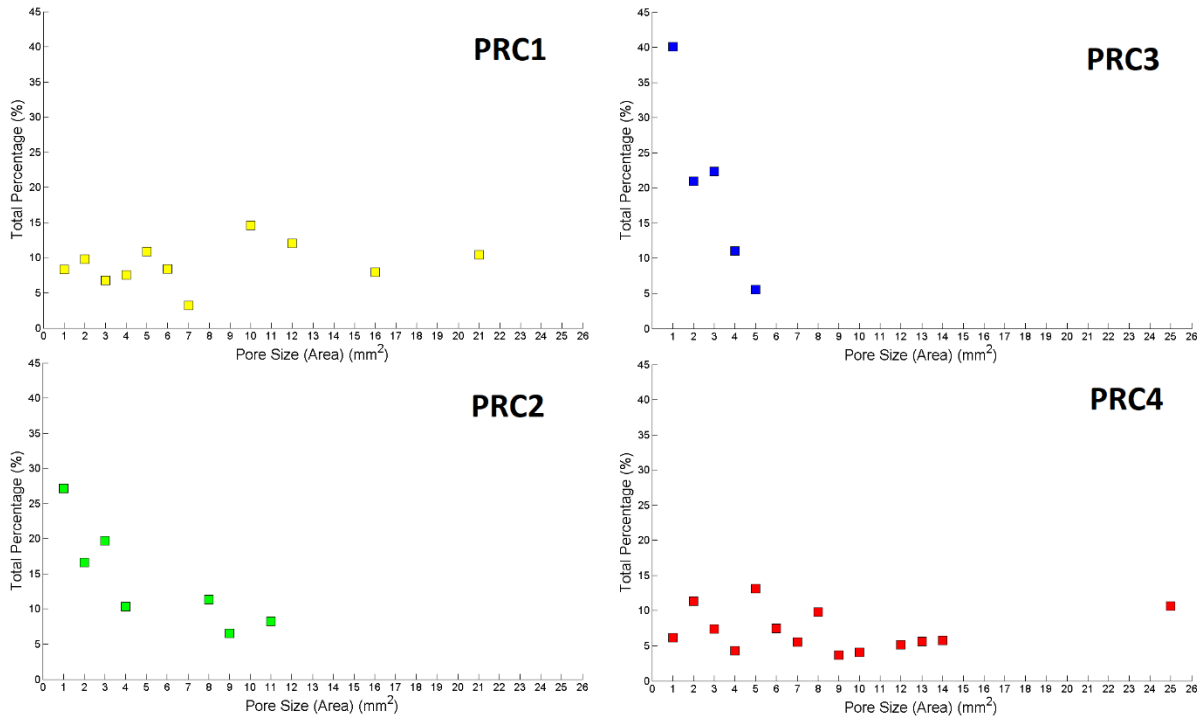Fig. 13. Determination of pore size distribution

Fig. 14. 2D pore size intervals versus cumulative percentage graph for PRC1, PRC2, PRC3 and PRC4

To have a clearer overview of the size distributions, the pores are grouped into size intervals. For example, pores with a size between 4 and 5 mm^2 are added up and collectively presented at pore size 5 in the graphs as seen in Fig. 14. The graphs demonstrate the pore size distributions of different mixtures. It can clearly be seen that PRC1 and PRC4 with 4-8 mm aggregates have larger pores compared to PRC2 and PRC3 with 2-4 mm and 50% 2-4 mm-50% 4-8 mm aggregates, respectively. The graphs show a tendency that the aggregate size affects the pore size distribution. The analyses provided complementary information to explain the impact strength results, as will be discussed in section 2.3.

2.3. Finite Element Analyses of Real Porous Concretes

In the analyses of real porous concretes, porous concretes were defined as four-phase materials consisting of aggregates, bulk cement paste, interfacial transition zones (ITZ) and meso-size arbitrarily shaped air pores. For the numerical analyses, the mixtures that have given the highest static and dynamic strengths while maintaining the multiple fragmentation behavior during the experiments were selected. Three porous concrete mixtures with basalt aggregates with different gradings (4-8 mm, 2-4 mm and 50% 4-8 mm-50% 2-4 mm), a 4-8 mm gravel aggregate porous concrete and a full concrete with 4-8 mm basalt aggregates were analyzed.

In the numerical analyses, the drop weight impact tests conducted on different types of porous concretes were simulated. The experimental impact tests were carried out using an instrumented drop-weight impact test set-up seen in Fig. 6. In the experiment, the specimen was placed vertically on a steel base structure, which also serves as a steel buffer plate that functions as a

16

wave sink at the impact experiments. The impactor was dropped from approximately 1.2 m to provide striking velocities ranging between 4.0 - 4.7 m/sec which were defined as initial velocity to the impactor in the numerical analyses. In the experiments, the selection of the impactor material and the magnitude of the impact velocity determine the pressure applied to the concrete sample. Therefore, by varying those properties, the input pressure could be controlled. The steel impactors used in the tests were 110 mm in diameter and 220 mm in height.

In the analyses, the aggregates were defined as linear elastic (with E=50 GPa, v=0.3 for basalt). The elastic constants to define the different gravel aggregates as well as their percentages are provided in Table 4.

Table 4. Percentages and material parameters of different gravel aggregates as applied in PRC4

Aggregate Type	Percentage (%) (based on number of elements)	E (GPa)	v
Sandstone	14.03	20	0.30
Feldspar	8.94	40	0.30
Limestone	19.56	27	0.25
Chert	6.22	65	0.20
Chalk	4.65	18	0.25
Quartzite	22.83	65	0.25
Granite	6.87	70	0.23
Basalt	16.88	50	0.25

The Concrete Damaged Plasticity (CDP) model, which is a plasticity-based damage model for concrete, was used to define the material properties of the cementitious phases that are present in the analyses, i.e. the interfacial transition zone (ITZ) and the bulk cement paste. The CDP model, that has been developed by Lubliner et al. and modified by Lee and Fenves, is an alteration and revision of the Drucker-Prager model [21-23]. It is a material model generally used for analyzing cementitious materials [24,25]. The model is based on the concepts of isotropic damaged elasticity and isotropic tensile and compressive plasticity to represent the inelastic behavior of concrete. In the model two main mechanisms are present, i.e. tensile cracking and compressive crushing. Different degradations of the elastic stiffness in tension and compression are considered. Rate sensitivity is also present. Especially an increase in the peak strength with strain rate can be captured [25-28]. For providing input data for the Concrete Damaged Plasticity Model, experimental stress-stain data (beyond the elastic range) was used as input in the analyses. The experimental data cannot however be used directly as input because even small fluctuations in the raw experimental graph may sometimes cause negative strain error during computation. Therefore, all the user-provided experimental stress versus inelastic strain data is smoothened and checked according to the format accepted by the program by taking the widely accepted works of Jankowiak and Lodygowski and Lubliner et al. in literature as reference [21, 25, 26].

The final meshes that have been generated with the mesh generation code were exported to the preprocessing software ABAQUS/CAE. A fixed boundary was defined at the bottom surface of the steel base structure. The displacement in x-direction and the rotation of the impactor were constrained in order to facilitate a purely vertical movement. In the drop weight experiments the same situation is valid because the drop weight travels down in a tube. Two (steel-concrete) contacts were defined between the steel base structure and the bottom surface of the concrete sample and between the steel impactor and the top surface of the sample. These surface-to-surface contacts had a friction coefficient of 0.3 in tangential direction. The (concrete-concrete) contacts formed between pore surfaces were defined as "self-contact" with a friction coefficient of 0.5 [29-31]. The presence of complex contact properties substantially decreases the time increment in the explicit computations. However, contacts are essential in conducting a realistic simulation for materials such as porous concrete. An impact velocity of 4.5 m/sec, which is approximately the velocity that had been measured during the laser Doppler velocimetry (LDV) experiments, was defined for the steel impactor. LDV was used in the experiments to record the real time velocity of the bottom surface of the impactor that is in contact with the concrete sample to derive the dynamic strength of the sample tested.

In Fig. 15, the impact stress time histories of the three porous concrete mixtures with basalt aggregates having gradings of 4-8mm (PRC1), 2-4 mm (PRC2) and 50% 4-8mm-50% 2-4 mm (PRC3), the 4-8 mm gravel aggregate porous concrete (PRC4) and the full concrete with 4-8 mm basalt aggregates (FC1) are presented.

When the peak values of the impact stress-time histories are checked and compared with the experimental results of the corresponding mixtures (in Table 3), it can be concluded that impact strengths of the samples obtained numerically are in a good agreement with the experimental results. While the results of PRC 1, PRC2 and PRC3 are closer to the experimental results, the numerically computed impact strength of PRC4 (gravel concrete) was slightly higher than the experimentally found value (see Table 3). This can be attributed to the fact that in the analyses of real porous concretes with basalt aggregate, the same material parameters were used while in porous concrete with gravel very different and varying material parameters had to be taken (see Table 4 and Fig. 11). Therefore, some of those parameters may have been assigned with inaccurate values. In addition, the percentages of the different types of gravel aggregates were intuitively selected in the analysis. The actual exact composition of the gravel aggregate batch could not be determined.
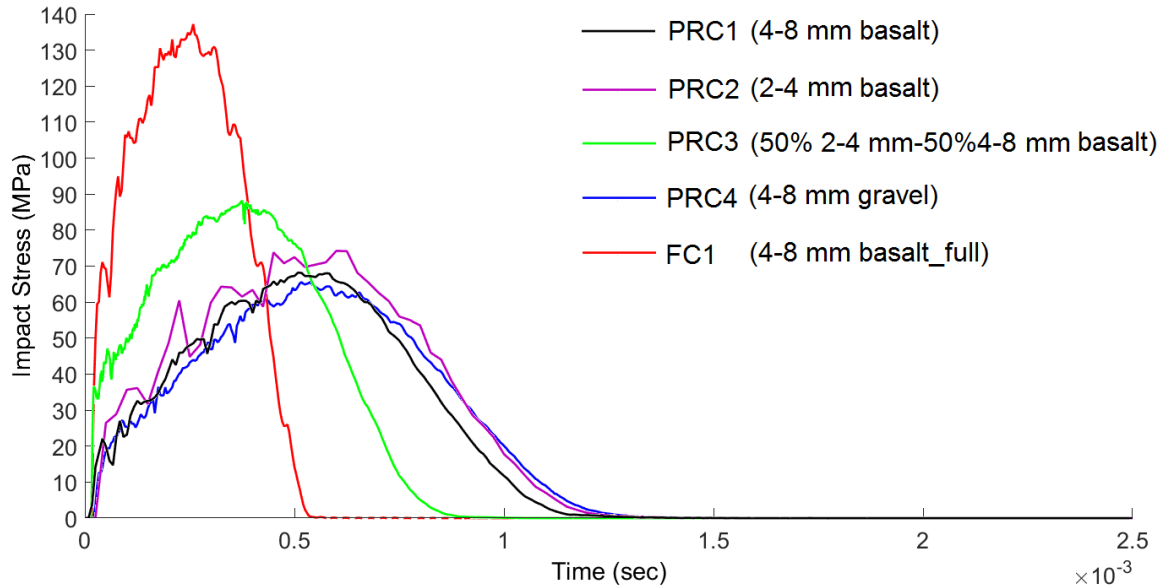
Fig. 15. Impact stress time histories for different porous concretes and a full concrete obtained from the numerical analyses

Similar to the experiments, highest impact strength among all the porous concrete mixtures was reached for 50% 4-8mm-50% 2-4 mm basalt porous concrete (PRC3). When the cementitious phase distributions (Fig. 12) and the pore size distributions (Fig. 13) of the different mixtures are also considered, it is seen that although the amount of ITZ is higher in mixtures containing finer (2-4 mm) basalt aggregates, those mixtures (PRC2, PRC3) had higher impacts strengths compared to the 4-8 mm aggregate mixture (PRC1). Contrary to the fact that ITZ is defined as the mechanically weakest phase among the three solid phases (aggregates, ITZ and bulk cement paste), PRC2, PRC3 mixtures providing higher impact strengths can be explained by the much finer pore structure of those mixtures.

It can be said that aggregate grading, which determines the porosity and pore size distribution of porous concretes, dominantly affects the strength and the fragmentation of the material. Numerical and experimental results show that if two sizes of aggregates (2-4 and 4-8 mm) are used instead of single sized aggregates, both the static compressive and the impact strengths of porous concretes increased. Therefore, PRC3, having aggregates of two sizes, is the mixture that reached the highest impact strength values in both analyses, i.e. about 86 MPa in the experimental and approximately 88 MPa in the numerical analyses. This can be attributed to the fact that an aggregate grading, that includes two different size ranges, provides a better packing and lower porosity. While a total porosity of 18.8% was measured on the experimental samples using image analysis (see Table 3 and Fig.4), in the numerical porosity calculations (Fig. 14), PRC3 had the smallest pore size distribution. Therefore, aggregate grading which determines the total porosity and the pore size distribution in porous concretes, was found to be the main factor that affects the strength. This can certainly be explained by the particles having varying sizes

being more densely packed. When compaction is applied, particles of different sizes pack even more densely as small particles move better into the voids between larger ones.

When the strengths of mixtures having single size aggregates (either 4-8 mm or 2-4 mm), i.e. PRC1 and PRC2 respectively, are compared, it can be said that as the aggregate size decreases (from 4-8 mm to 2-4 mm) the strengths very slightly increase. When the porosity values of the mixtures are compared, it is seen that the total porosities of mono-sized aggregate mixtures are almost the same, irrespective of the aggregate size. Therefore, the slight increase in strengths can be explained by the decrease in pore size distribution (Fig. 14) and the increase in contact or bonding areas with decreasing size of the aggregates.

If the mixtures having the same aggregate size compositions, but different types of aggregates (PRC1 and PRC4) are compared (i.e. river gravel was used in PRC4 instead of crushed basalt), a slight decrease is seen in the numerical results with the use of gravel while the decrease in experimental results was more pronounced. River gravel tends to have a more equi-dimensional and rounded shape compared to crushed basalt which is more elongated and angular. Crushed aggregates not only have irregular shapes, but also have a rough texture. Due to these differences in shape and texture, the river gravel facilitates a better packing. Therefore, mixtures incorporating river gravel (PRC4) have a 17.9 % porosity, which is lower than those of the mixtures with basalt. On the contrary, a rough texture and high angularity contribute to porous concrete strength due to enhanced mechanical interlock, increased total surface area and increased contact points. In meso-scale testing, it was also found that the different mineralogical types of rocks present in river gravel have very different levels of adherence to cement paste, which was also implemented as a factor in the numerical analyses of PRC4.

When all the curves obtained from different mixtures are compared, it can be observed that in full concrete (FC1), the peak stress is reached in a shorter time and a faster failure is evident, as expected.

Since one of the main objectives of the numerical research was estimating the fragmentation behavior of porous concrete, the damage contours of the analyzed concretes were also evaluated. When the compressive and tensile damage contours of a 2-4 mm basalt aggregate porous concrete are examined by zooming into one of the pores (see Fig 16), it can be seen that the top and bottom poles of the pores suffer from tensile damage. Compressive damage occurs more at the sides of the pores and at the triaxially confined zones above and below the aggregates. At those locations, similar to the triaxially confined zones at the top and bottom borders of the specimen, the lateral expansion of cement paste is restraint by the aggregates and triaxial compression develops at the top and bottom of the aggregates [32, 33].
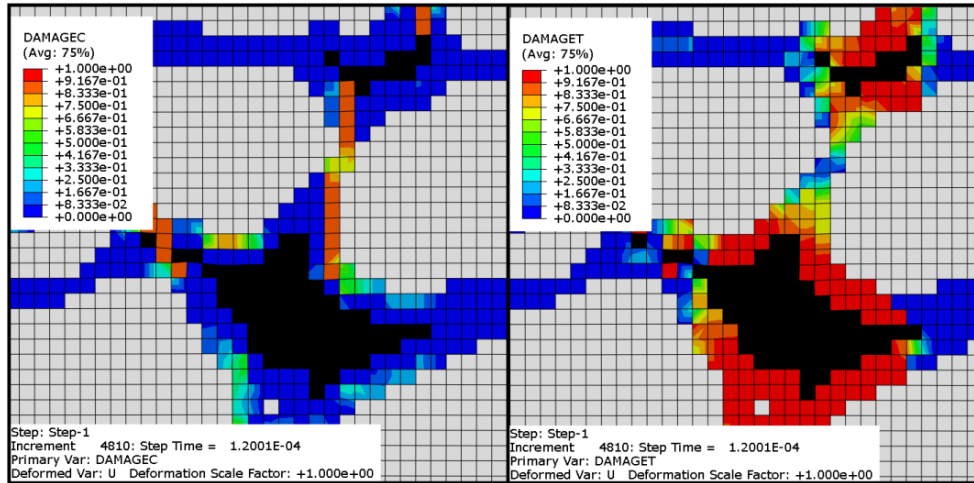
Fig. 16. Compressive (left) and tensile (right) damage contours around a pore (PRC3) (Damage for each stress condition (C or T) is represented by a scalar value that ranges between 0 to 1)

When a larger mesh area is analyzed, the same types of damage are seen throughout the concrete (see Fig. 17). Additional concentrations of splitting tensile damage can also be seen between the aggregates in the vertical direction. Immediately above and below the aggregates and also at the diagonal contact points, the compressive damage is also evident.
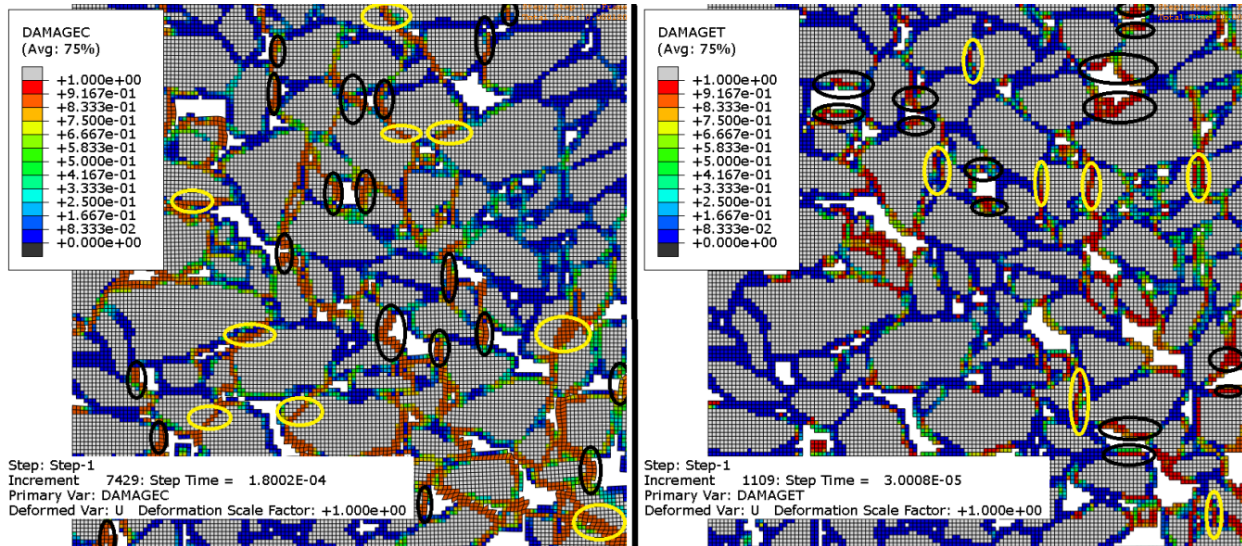

Fig. 17. Distributions of compressive (left) and tensile (right) damage contours (PRC3)
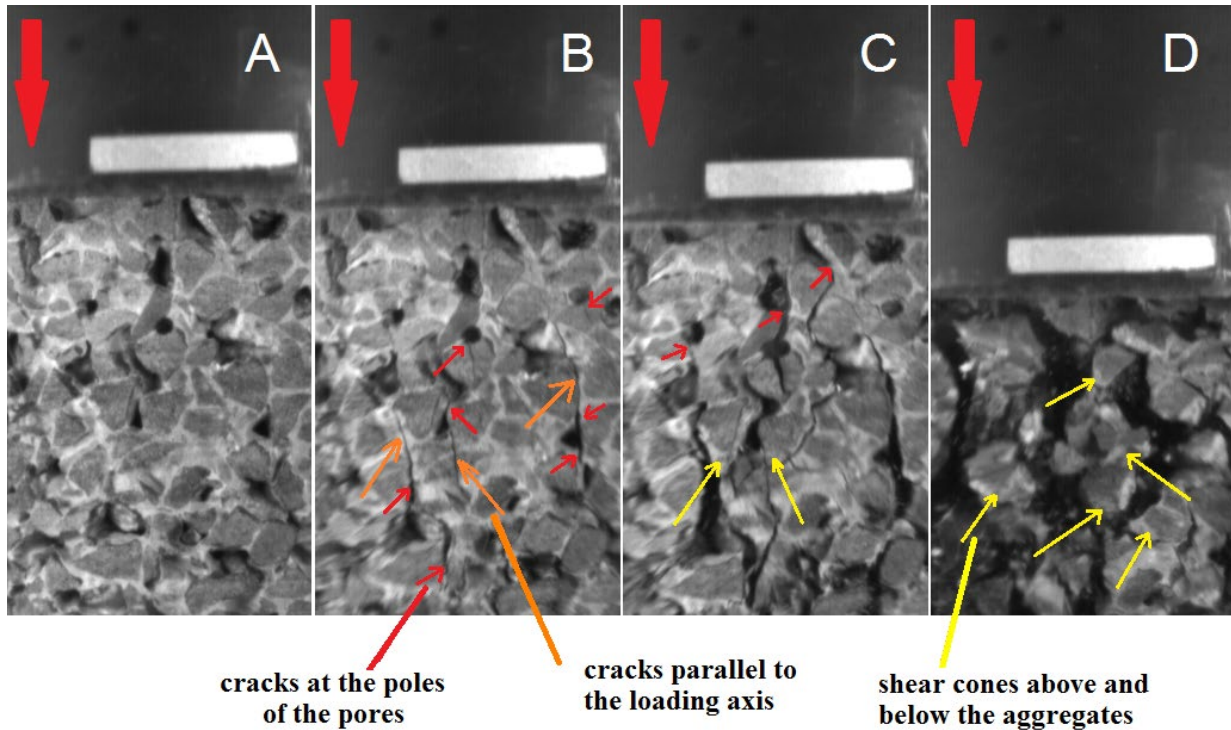
Fig. 18. High speed photographs for the impact test of a 4-8 mm basalt aggregate porous concrete sample demonstrating the fracture patterns

The numerical results have also been compared with the images acquired using high speed photography. In Fig. 18, crack patterns such as tensile cracks parallel to the axis of loading (indicated by orange arrows) and the subsequent shear cones underneath the aggregates (indicated by yellow) can be observed. On the other hand, due to the porous structure, cracks initiating from the upper and lower poles of the pores (indicated by red arrows), where tensile stress concentrations are present, are also evident. Similar crack distributions were also observed in the numerical results (in Fig 17).

After examining the locations of tensile and compressive damage concentrations individually, the complete samples were examined at different times. For each mixture, two pictures were presented ($2.5*10^{-4}$ sec which is much earlier than the peak and $1.5*10^{-3}$ sec which is after the peak) in Figs. 19-23. The elements that correspond to a tensile or compressive damage value of 0.9 or higher were removed in order to estimate the crack patterns and fragment sizes. From the images at $2.5*10^{-4}$ sec, it is evident that some cracks are initiated and formed much earlier than when the peak strength is reached.
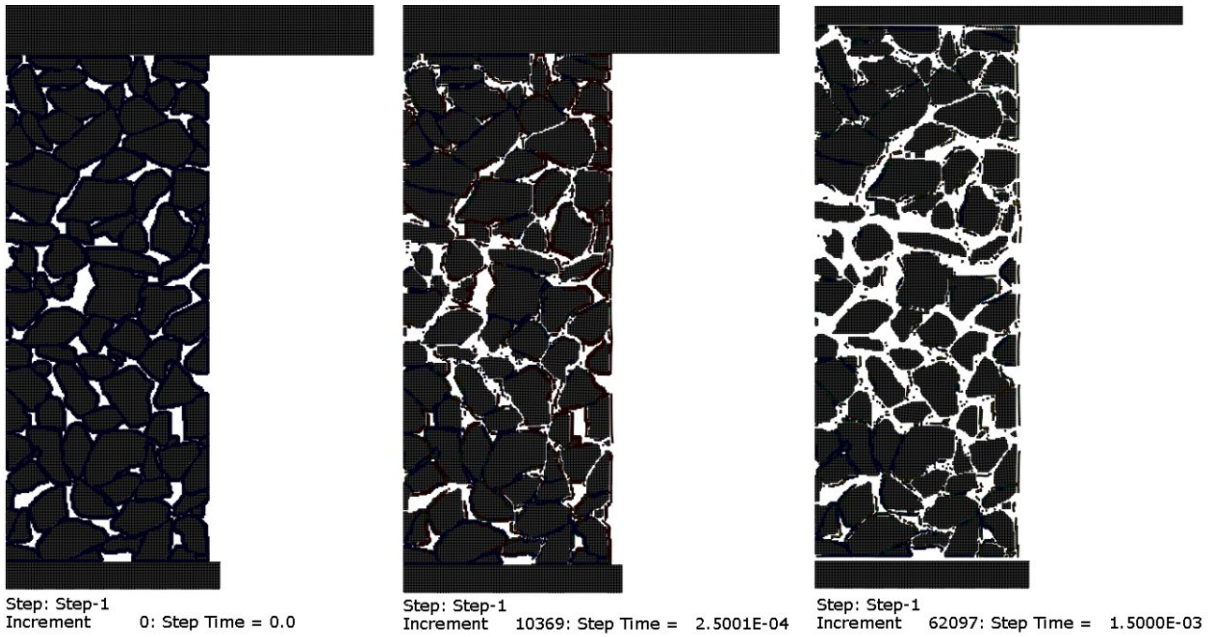
Fig. 19. Compressive + tensile damage variable contours in PRC1 (with 4-8 mm basalt aggregates) (elements having DamageC or DamageT ≥ 0.9 removed.)
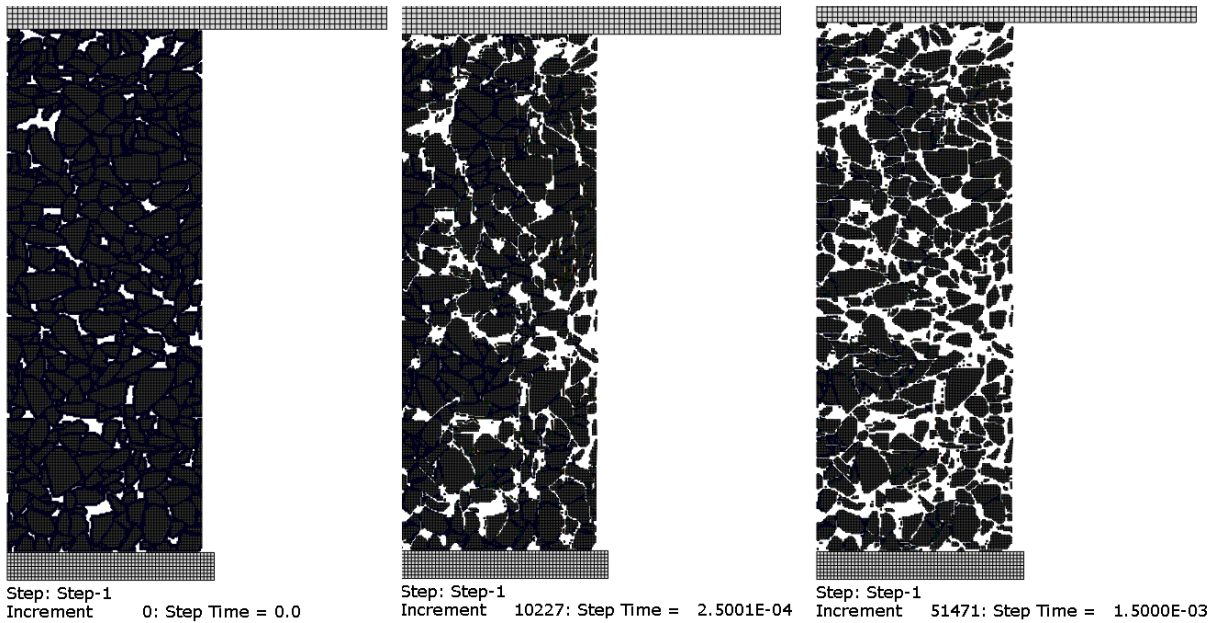

Fig. 20. Compressive + tensile damage variable contours in PRC2 (with 2-4 mm basalt aggregates) (elements having DamageC or DamageT ≥ 0.9 removed.)

Step: Step-1
Increment   0: Step Time = 0.0

Step: Step-1
Increment   7123: Step Time =   2.5001E-04

Step: Step-1
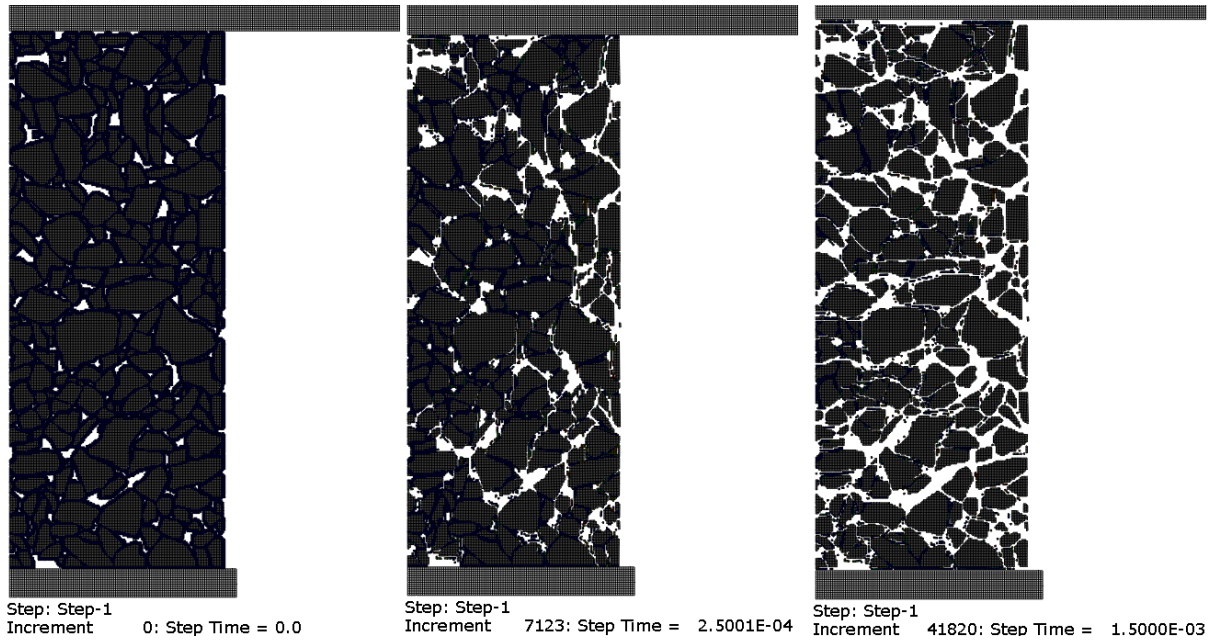Increment   41820: Step Time =   1.5000E-03

Fig. 21. Compressive + tensile damage variable contours in PRC3 (with 50% 2-4 mm-50% 4-8 mm basalt aggregates) (elements having DamageC or DamageT $\geq$ 0.9 removed.)

Step: Step-1
Increment   0: Step Time = 0.0

Step: Step-1
Increment   10540: Step Time =   2.5001E-04

Step: Step-1
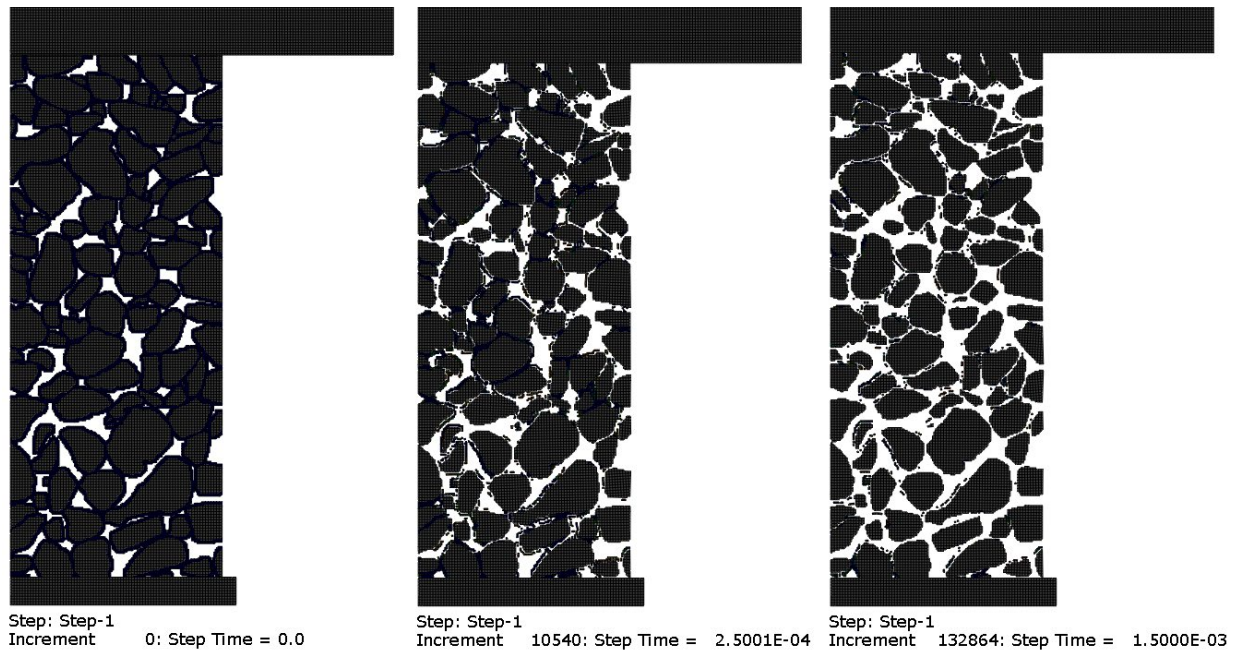Increment   132864: Step Time =   1.5000E-03

Fig. 22. Compressive + tensile damage variable contours in PRC4 (with 4-8 mm gravel aggregates) (elements having DamageC or DamageT $\geq$ 0.9 removed.)
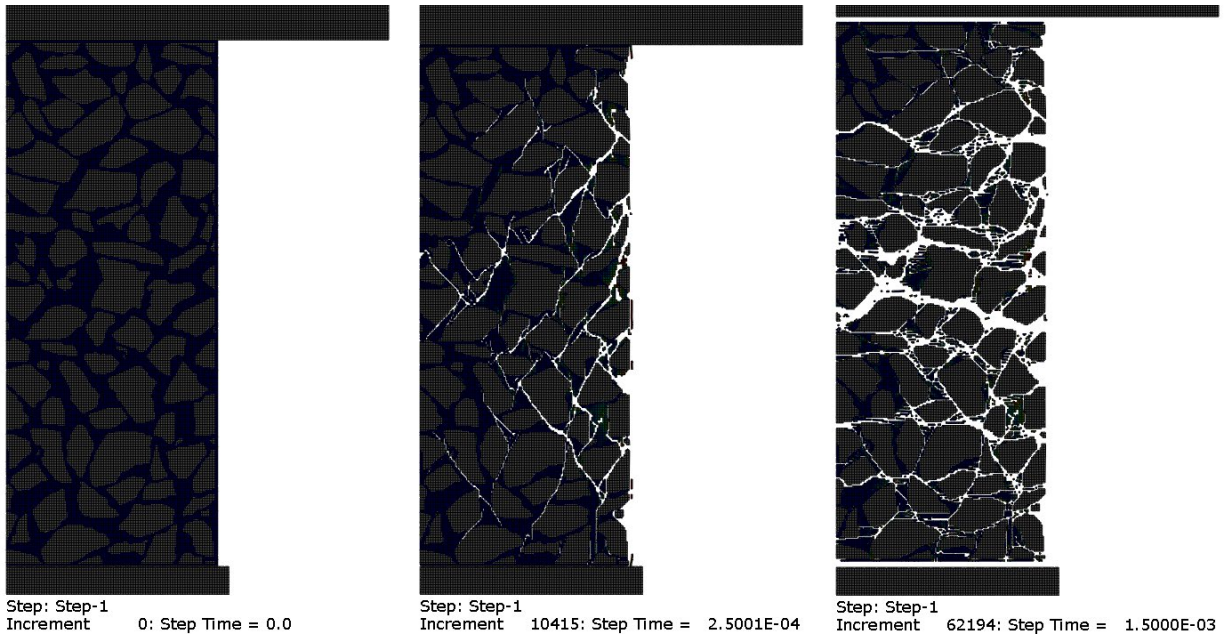
Step: Step-1
Increment   0: Step Time = 0.0

Step: Step-1
Increment   10415: Step Time = 2.5001E-04

Step: Step-1
Increment   62194: Step Time = 1.5000E-03

Fig. 23. Compressive + tensile damage variable contours in FC1 (4-8 mm basalt aggregate full concrete) (elements having DamageC or DamageT ≥ 0.9 removed.)

In the damage contours in Figs. 19-22, the elements that have reached a damage parameter (either compressive DamageC or tensile DamageT) value of 0.9 under impact loading have been removed. Tensile damage occurs much earlier in time than compressive damage in concrete (under compressive loading) due to the tensile strength of cementitious materials being significantly lower than their compressive strength. This can also be sensed from the timings of Fig. 17 where a siginificant amount of tensile damage (on the right) is observed in much earlier in time than a similar amount of damage is seen in terms of compressive damage (on the left). Therefore, tensile damage is more dominantly observed in the samples in Figs. 19-22 under impact loading.

If the images are compared, it is clear that the mixtures with 4-8 mm (basalt or gravel) aggregates (PRC1 and PRC4) fractured into fragments nearly in the size of their aggregates. In PRC2, containing 2-4 mm aggregates, fragments were small compared to PRC1 and PRC4 due to the small sized aggregates. In all mixtures, at a few locations, aggregates were bound to each other and stayed intact in groups. These locations are mostly in the triaxially confined zones at the borders of the samples. This is similar to what was also observed during the experimental impact tests. Since in the computations realistic boundary conditions and friction coefficients are defined, structural affects such as triaxial confinement at the boundaries, that occur during the experiments, are also experienced in the numerical analyses. When the porous concretes are compared (Figs. 19-22) with the full concrete (Fig. 22), the multiple fracturing performance of porous concretes can be distinguished. The small bridges that assemble the aggregates in porous concretes were easily broken and the samples fractured into fragments nearly as small as their aggregates. Full concrete on the other hand, fractured into larger size fragments.

The fragmentation performances of different porous concrete mixtures strongly depend on the aggregate grading. Smaller size aggregates (i.e. 2-4 mm) facilitate the formation of smaller size fragments. However, for those aggregates, the amount of contact surface between the neighboring aggregates (per aggregate volume) is higher. Therefore, small aggregates are bonded more strongly with their neighbors. This causes some locally larger fragments in mixtures containing 2-4 mm aggregates. Therefore in selecting a mixture among the ones that have been analyzed, i.e. PRC1, PRC4 (mixtures with sufficient static strengths and nearly no large-size fragments) and PRC2, PRC3 (mixtures having higher strengths and fragments that generally smaller, but locally larger than those of PRC1 and 4) should be evaluated according to the strength requirements of that specific application. If porous concretes are generally compared with the full (FC1) and the normal (NC1) concrete mixture, the difference is extensive. In the numerical as well as experimental results, the full concrete (a type of high strength concrete obtained by completely filling the pores of porous concrete with cement paste) showed a very different fracturing behavior where the fragments were very large. In the drop weight impact experiments, the moderate strength normal concrete (NC1), which had about the same strength as a typical moderate strength porous concrete e.g. PRC1, did not fracture into small fragments while PRC1 fractured into fragments at nearly the size of its aggregates (see Fig. 24) [5]. This showed the benefits of using highly compacted, enhanced strength porous concretes in safety applications that require multiple fragmenting.
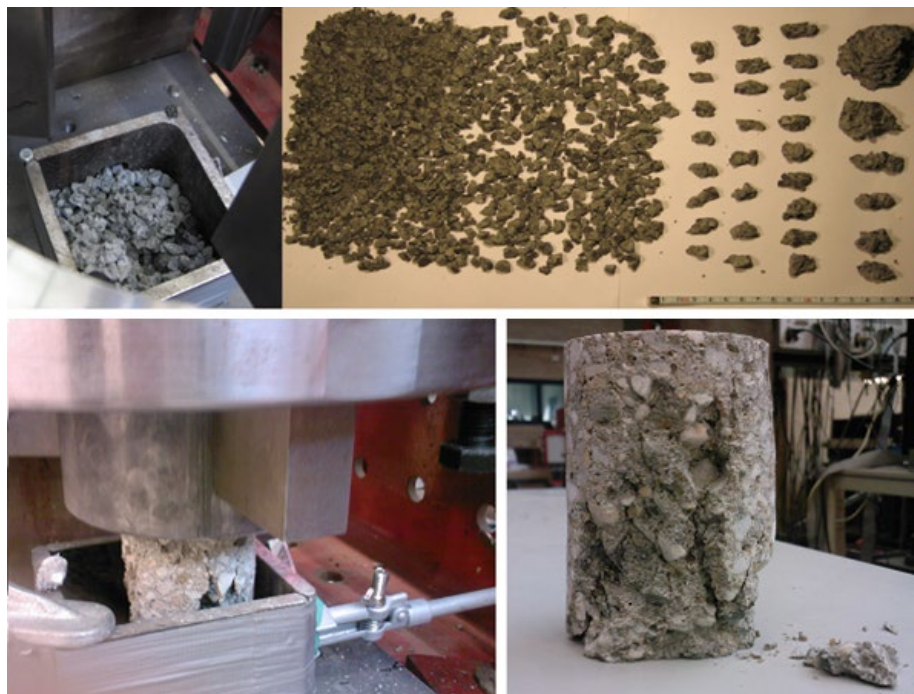

Fig.24. Post-failure fragments of a porous (PRC1) (top) and a normal concrete (NC1) (bottom) after a drop weight impact test

2.4. Fragment Size Distribution Analysis

Damage evolution contours (in Figs. 19-22) give an impression about the crack patterns, that may be expected to form in the impact testing of porous concretes, and may be used in estimating the fragment sizes. In the analyses, highly damaged (damage parameter $\geq$ 0.9) elements were again removed (see also Fig. 25). The same analysis that was conducted to quantify the pore data was conducted on the fragments. An example is presented in Fig. 25. Because an axisymmetric analysis was performed, the areas of the fragments that are intersecting the axis of symmetry (y-axis or x=0) were doubled (see the red bordered fragments in Fig. 26). Meanwhile, the rest of the fragments (see the blue bordered fragments Fig. 26) were taken to be present two times.
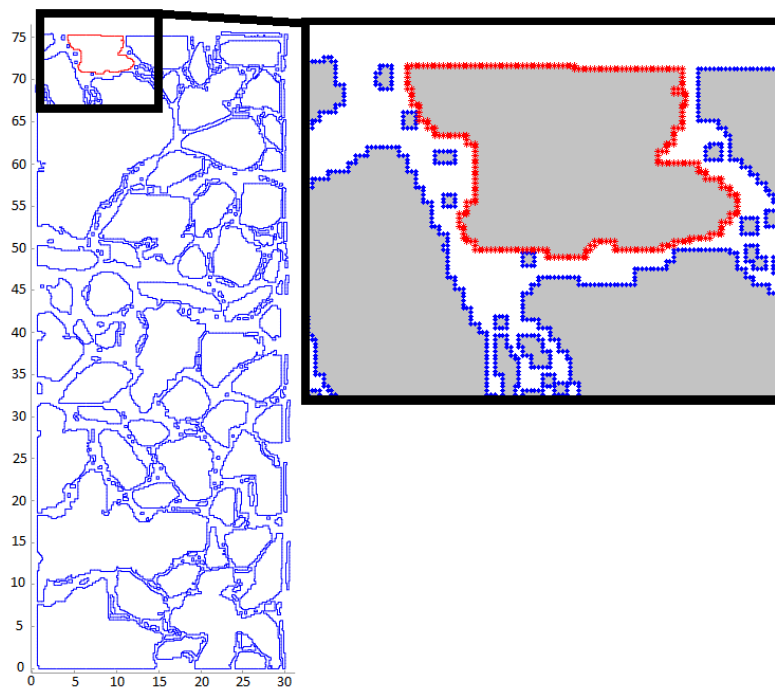

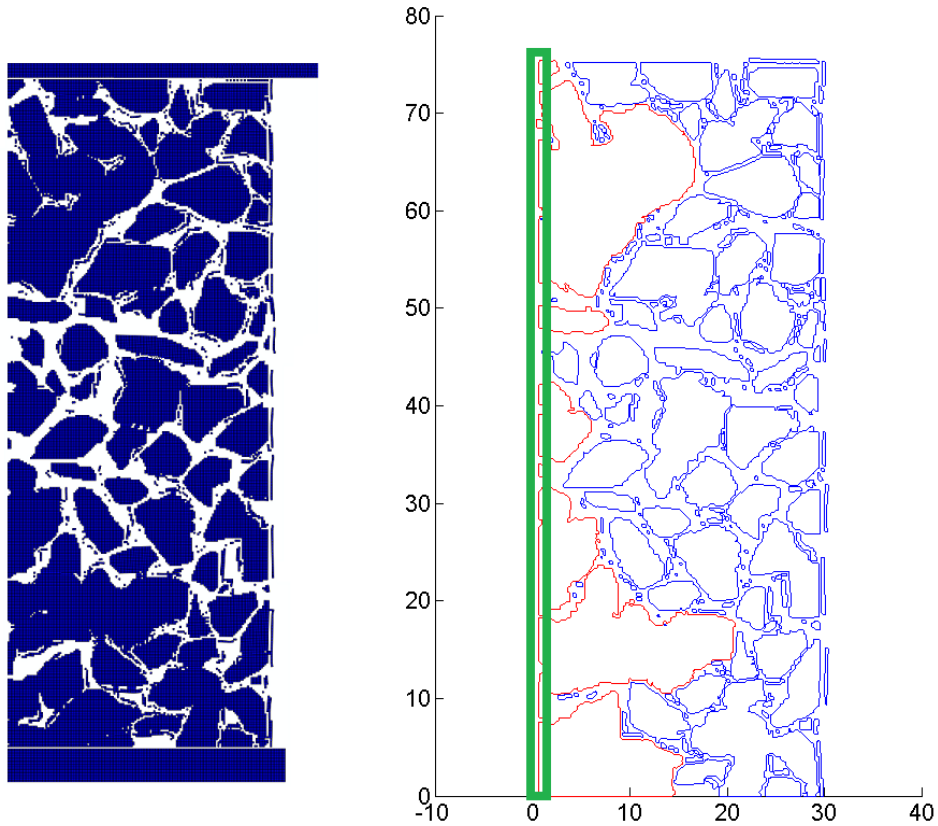Fig. 25. Determination of fragment sizes

Fig. 26. The fragments with doubled areas (red) due to axisymmtery (intersecting the y-axis)

The individual 2D sizes were again grouped into size intervals as previously done in pore size analyses. During the actual drop weight experiments, in order to quantify the sizes of the fragments, the tests were done in a closed environment and all the fragments were collected. The collected fragments have been sieved through standard sized sieves and their sizes were quantified in terms of the sieve opening sizes. The numerical results could therefore be compared with the sieve analysis results by this time converting the 2D sizes (areas of the fragments in Fig. 27) from the numerical analysis to standard sieve sizes. This was done by calculating the diameters of the circles having the same corresponding areas and again grouping them in terms of the sizes of the standard sieves starting from 4 mm (i.e. 4, 8,16 and 32 mm). The bar graph in Fig. 28 shows the two sets of results both expressed in terms of standard sieve sizes. The numerical fragment size analysis seems to estimate the fragment sizes quite sufficiently up to 16 mm, but slightly deviates from the experimental results at the larger size fragments.
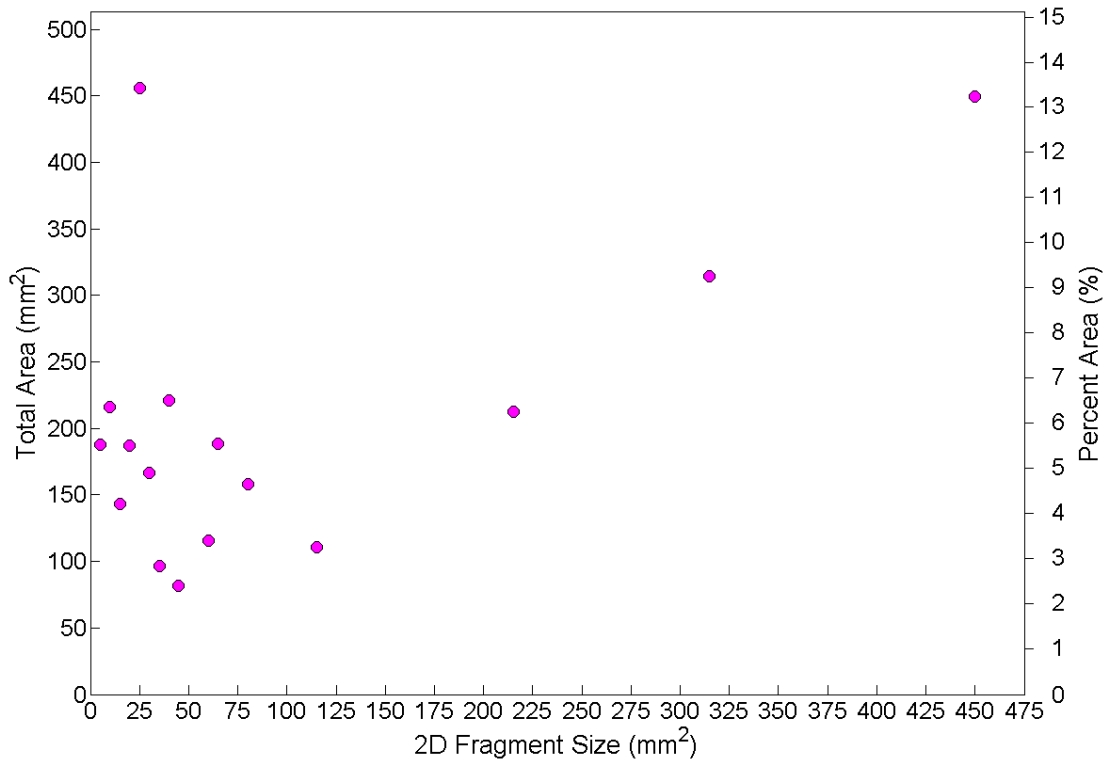
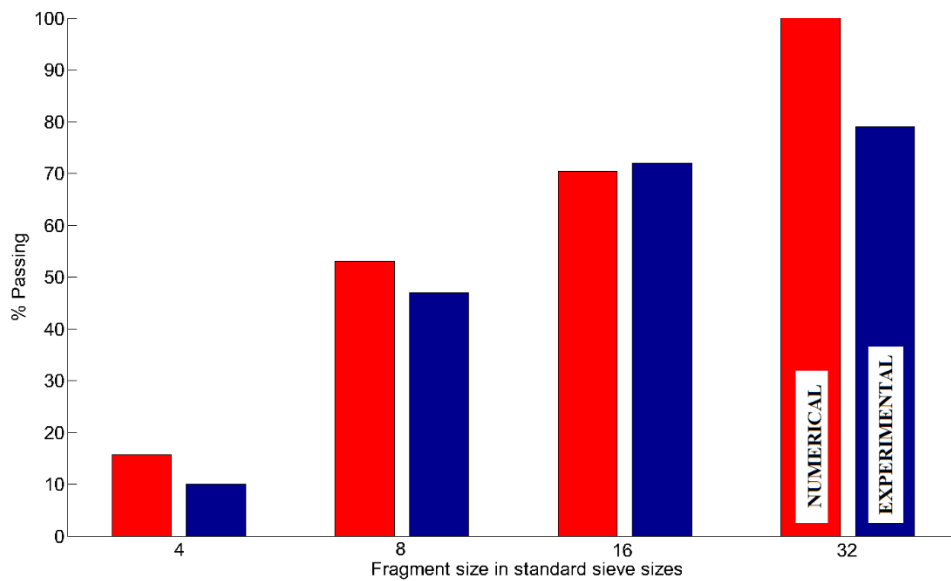Fig. 27. 2D fragment size intervals versus cumulative area and percentage graph for PRC1

Fig. 28. Comparison of the numerical and experimental fragment sizes in terms of standard sieve sizes

3. Conclusions

In this research article, the dynamic behaviors of different porous concretes, that have been experimentally produced and tested under drop weight impact loading, were numerically simulated and assessed. The following conclusions can be drawn regarding this numerical study:

- In the analyses, porous concrete was identified at the meso-scale as a four phase material consisting of aggregates, interfacial transition zones (ITZ), bulk cement paste and air. By defining each material phase separately based on experimental input, different types of porous concretes were modeled and compared with experimental results.
- For the realistic representation of the real porous concretes that have been tested, the aggregates were directly determined through 3D computed tomography. The mesh generation program, that has been developed, provided finite element meshes that resemble real porous concretes and the phase distributions were close to those of actual materials.
- Numerical analysis of the pore and fragment size distributions provided complementary information to better understand the dynamic behavior of the different mixtures. As the size of the aggregates included in the mixture was decreased, finer pore structures could be obtained. The fragmentation behavior of the porous concretes obtained from numerical analyses were consistent with the experimental results.
- According to all the numerical and experimental results obtained, it can generally be concluded that aggregate grading which is very effective in the formation of the skeleton structure of the material, determines the porosity and pore size distribution of porous concretes and thus dominantly affects the strength and the fragmentation of porous concrete.
- Both numerical and experimental results showed that when more than one size of aggregates were used instead of single sized aggregates, both the static compressive and the impact strengths of porous concretes increased. Among the investigated porous concrete mixtures, the mixture having aggregates of two sizes, was the mixture that reached the highest impact strength values in all analyses. This can be attributed to the fact that the grading, that includes two aggregate sizes, provides a better packing and consequently a lower porosity. When compaction is applied, particles of different sizes pack even more densely as small particles flow better into the voids between larger ones. A denser packing leads to a lower total porosity and a finer pore structure, which was also recognized in the numerical porosity calculations.
- When the impact strengths of mixtures having single size aggregates (either 4-8 mm or 2-4 mm) are compared, it can be concluded that as the aggregate size decreases (from 4-8 mm to 2-4 mm) the strengths slightly increase. When the porosity values of the mixtures are compared, it is seen that the total porosities of mono-sized aggregate mixtures are almost the same, irrespective of the aggregate size. Therefore, the slight increase in strengths can be explained by the decrease in pore size and the increase in contact or bonding areas (per aggregate volume) with decreasing size of the aggregates.
- If the mixtures having the same aggregate grading, but different types of aggregates i.e. river gravel or crushed basalt, are compared in terms of their strengths, a slight decrease in the numerical results was found for river gravel. The decrease in experimental results was more pronounced. River gravel tends to have a more equi-dimensional and rounded shape compared to crushed basalt. Owing to its shape and smooth texture, river gravel facilitates a better packing. Therefore, mixtures incorporating river gravel had a lower porosity compared to those having crushed basalt. On the contrary, rough

texture and high angularity contribute to strength due to enhanced mechanical interlock, increased total surface area and increased contact points. On the other hand, in meso-scale testing, it was found that different types of rocks also have very different levels of adherence to cement paste, which was also implemented in the numerical analyses. Mineralogically different aggregates also certainly have different mechanical properties themselves. Due to all the mentioned factors involved, the porous concrete with river gravel had a lower static and impact strength compared to crushed basalt porous concretes.

- The fragmentation performances of different porous concrete mixtures also strongly depend on aggregate grading. While smaller size aggregates facilitate the formation of smaller size fragments, for those aggregates, the amount of contact surface (per aggregate volume) between particles is higher. This causes some locally larger fragments in mixtures containing smaller aggregates while those mixtures also generally show higher strength. Thus, in choosing a mixture to be used in safety structures, the selection should be done in view of the service loads and the amplitude of impact stress the concrete is expected to be exposed to in that specific application. For increasing the strength, the pore size, which is determined by the aggregate size, should be refined. Therefore, aggregate size should either be decreased or more than one size of aggregates should be used. Decreasing the aggregate size generally works in favor of multiple cracking and therefore mostly decreases the fragment size while some locally larger fragments also exist.

- It was seen in both the numerical and the experimental analyses that, porous concretes have a very different fracturing behavior compared to concretes without meso-size pores. In porous concretes, cracks are forced to propagate into locations guided by the aggregate skeleton structure and the pore distribution. When porous concretes are generally compared with concretes without meso-size pores, the difference in fragmentation is very evident. According to the numerical as well as experimental results, in the concretes without meso-size pores the fragments formed were very large. In the drop weight impact experiments, the moderate strength normal concrete (NC1), which had about the same strength as a typical moderate strength porous concrete, did not fracture into small fragments while a similar strength porous concrete e.g. PRC1, fractured into fragments at nearly the size of its aggregates. These results showed the benefits of using highly compacted, enhanced strength porous concretes in safety applications, which require a building material that fractures into small fragments under impact loading.

Acknowledgement

References

[1] M. Lukovic, H. Dong, B. Šavija, E. Schlangen, G. Ye, K. van Breugel, Tailoring strain-hardening cementitious composite repair systems through numerical experimentation, Cem. and Conc. Comp. 53 (2014) 200-213.

[2] X. Ouyang, G. Ye, K. van Breugel, Experimental and numerical evaluation of mechanical properties of interface between filler and hydration products, Construct. and Build. Mat. 135 (2017) 538–549.

[3] Z. Qian, E. Schlangen, 3D modeling of fracture in cement-based materials, J. Multiscale Modelling 1(2) (2009) 245-261.

[4] R.R. Pedersen, A. Simone, L.J. Sluys, Mesoscopic modeling of concrete under different moisture conditions and loading rates, in: J.Weerheijm (Eds.), Undertstanding the Tensile Properties of Concrete, Woodhead Publishing, Cambridge, 2013, pp. 268-293.

[5] A.S. Agar Ozbek, Design and Analyses of Porous Concrete for Safety Applications, Delft University of Technology, 2016.

[6] J.T. Kevern, V.R. Schaefer, K. Wang, Evaluation of pervious concrete workability using gyratory compaction, J. of Mat. in Civ. Eng., 21(12) (2009) 764-770.

[7] N. Ghafoori, S. Dutta, Development of no-fines concrete pavement applications, J. Transport Eng 121(3) (1995) 283–8.

[8] N. Ghafoori, S. Dutta, Building and nonpavement applications of no-fines concrete, J. of Mat. in Cvl. Eng. 7(4) (1995) 286-9.

[9] R. Zhong, K. Wille, Material design and characterization of high performance pervious concrete, Cons. and Build. Mat.98 (2015) 51–60.

[10] W.D. Martin, N. B. Kaye, B. J. Putman, Impact of vertical porosity distribution on the permeability of pervious concrete, Cons. and Build. Mat. 59 (2014) 78-84.

[11] J. Yang, G. Jiang, Experimental study on properties of pervious concrete, Cem. and Conc. Res., 33(3) (2003) 381-6.

[12] S.R. Wu, L. Gu, Introduction to the Explicit Finite Element Method for Nonlinear Transient Dynamics, John Wiley and Sons, New Jersey, 2012.

[13] R. De Borst, M. A.Crisfield, J.J.C. Remmers, C.V. Verhoosel, Non-linear Finite Element Analysis of Solids and Structures, John Wiley and Sons, West Sussex, 2012.

[14] G. Noh, K.J. Bathe, An Explicit Time Integration Scheme for the analysis of wave propagations, Computers and Structures 129 (2013), 178–193.

[15] N.S. Tarque, Numerical modelling of the seismic behavior of adobe buildings, PhD Thesis, (2011) University of Pavia, Italy.

[16] U. Farooq, K. Gregory, Explicit dynamic simulation of drop-weight low velocity impact on carbon fibrous composite panels, ARPN Journal of Engineering and Applied Sciences 5(3) (2010) 50-61.

[17] C.C. Huang, T.Y. Wu, A study on dynamic impact of vertical concrete cask tip-over using explicit finite element analysis procedures, Annals of Nuclear Energy 36(2) (2009) 213–221.

[18] W. Elmer, E. Taciroglu, L. McMichael, Dynamic strength increase of plain concrete from high strain rate plasticity with shear dilation, International Journal of Impact Engineering 45 (2012) 1–15.

[19] A.S. Agar Ozbek, J. Weerheijm, E.Schlangen, K. van Breugel, Investigating porous concrete with improved strength: testing at different scales, Construction and Building Materials 41 (2013) 480-490.

[20] A.S. Agar Ozbek. J. Weerheijm, E. Schlangen, K.van Breugel, Dynamic behavior of porous concretes under drop weight impact testing, Cement and Concrete Composites 39 (2013) 1-11.

[21] J. Lubliner, J. Oliver, S. Oller, E. Oñate, A plastic-damage model for concrete, International Journal of Solids and Structures, 25(3), (1989), pp. 229-326.

[22] J. Lee, G.L. Fenves, A plastic damage model for cyclic loading of concrete structures, ASCE Journal of Engineering Mechanics 124 (1998) 892–900.

[23] A. Hillerborg, M. Modeer, P. E. Petersson, Analysis of crack formation and crack growth in concrete by means of fracture mechanics and finite elements, Cem. and Conc. Res. 6 (1976) 773–782.

[24] S.V. Chaudhari, M.A. Chakrabarti, Modeling of concrete for nonlinear analysis using finite element code ABAQUS, Int. J. of Comp. Appl. 44(7) (2012) 14-18.

[25] Simulia_1 (2013), ABAQUS Analysis User's Manual 6.13.

[26] T. Jankowiak, T. Lodygowski, Identification of parameters of concrete damage plasticity constitutive model, Foundations of Civil and Environmental Engineering 6 (2005) 53-69.

[27] P. Kmiecik, M. Kaminski, Modelling of reinforced concrete structures and composite structures with concrete strength degradation taken into consideration, Archives of Civil & Mechanical Engineering 11(3) (2011) 623-636.

[28] Martin, O. Comparison of different constitutive models for concrete in ABAQUS/Explicit for missile impact analyses, Joint Research Center (JRC) European Commission, The Netherlands, 2010.

[29] N.J.S. Gorst, S.J. Williamson, P.F. Pallett, L.A Clark, Friction in temporary works, Research Report, University of Birmingham, U.K., 2003.

[30] Deutsches Institut für Normung, Falsework calculation, design and construction DIN 4421:1982, Beuth Veriag GmbH, Berlin, Germany, 1982.

[31] British Standards Institution, Falsework performance requirements and general design, Draft prEN 12812, London, U.K., 1997.

[32] P. Stroeven, Some aspects of the micromechanics of concrete, PhD Thesis, Delft University of Technology, the Netherlands, 1973.

[33] J.G.M. van Mier, Fracture Processes of Concrete: Assessment of Material Parameters for Fracture Models, CRC Press, USA, 1997.